Auxin molecular field maps define AUX1 selectivity: many auxin herbicides are not substrates

Klara Hoyerova[1*], Petr Hosek[1*], Mussa Quareshy[2*], Jun Li[3], Petr Klima[1], Martin Kubes[4], Antony A Yemm[2], Paul Neve[5], Ashutosh Tripathi[2], Malcolm J Bennett[6] and Richard M Napier[2]

[1] Institute of Experimental Botany, Academy of Sciences of the Czech Republic, Rozvojova 263, 165 02 Prague 6, Czech Republic; [2]School of Life Sciences, University of Warwick, Gibbet Hill Road, Coventry, CV4 7AL, UK; [3]Department of Pesticide Science, College of Crop Protection, Nanjing Agricultural University, Weigang 1, Nanjing, Jiangsu Province, P.R. China; [4] Centre of the Region Haná for Biotechnological and Agricultural Research, Department of Chemical Biology and Genetics, Šlechtitelů 241/27, 78371 Olomouc, Czech Republic; [5]Rothamsted Research, Harpenden, UK; [6] Plant Sciences Division and Centre for Plant Integrative Biology, School of Biological, Sciences, The University of Nottingham, Sutton Bonnington Campus, Loughborough, LE12 5RD, UK

[*] these authors contributed equally to the work

Author for corresondence: Prof Richard Napier
Tel: ++44 (0)24 765 75094
e-mail: richard.napier@warwick.ac.uk

Total word count	5379	No. of figures	7 (all colour except Fig.2)
Summary	199	No. of Tables	3
Materials and Methods	689	N. of Supporting Information files:	14 (Fig. S1-S11; Table S1-2; Method M1)
Results	3185		
Discussion	1279		
Acknowledgements	27		

Twitter: To follow

Short version of title: AUX1 substrate pharmacology

Funding sources:

RMN acknowledges support from BBSRC via grants BB/L009366 and BB/I023933/1 and an MIBTP studentship to MQ. AY was supported by a studentship from the Biotechnology and Biological Sciences Research Council, UK. KH was supported by the Czech Science Foundation, project no. 16-19557S; by MEYS of the Czech Rep., project no. LD 15137; and by the EU Operational Programme Prague – Competitiveness, project no. CZ.2.16/3.1.00/21519: Modern instruments for plant research. AT was supported by the Association of Commonwealth Universities award CP-2013-37

Author contributions:

The root growth bioassays were done by MQ, JL, AY and AT; the radiolabel uptake assays were done by KH, PH, PK, MK and RN. The concept of evaluating substrate selectivity by differential bioassay was developed by AY, MB and RN and the extension to additional herbicides by PN, RN and KH. The analysis using Forge software and molecular field point mapping was done by MQ. The manuscript was prepared by RN and all the authors contributed to editing and the final version.

Single sentence summary:

We have mapped the molecules carried by the auxin uptake carrier AUX1 and developed a picture of allowable substrates. We find that many synthetic auxin herbicides are not accumulated through this transporter.

Summary

(1) Developmental responses to auxin are regulated by facilitated uptake and efflux, but detailed molecular understanding of the carrier proteins is incomplete.

(2) We have used pharmacological tools to explore the chemical space that defines substrate preferences for the auxin uptake carrier AUX1. Total and partial loss-of-function *aux1* mutants were assessed against wild-type for dose dependent resistance to a range of auxins and analogues. We then developed an auxin accumulation assay with associated mathematical modelling to enumerate accurate IC_{50} values for a small library of auxin analogues. The structure activity relationship data was analysed using molecular field analyses to create a pharmacophoric atlas of AUX1 substrates.

(3) The uptake carrier exhibits a very high level of selectivity towards small substrates including the natural indole-3-acetic acid, and the synthetic auxin 2,4-dichlorophenoxyacetic acid. No AUX1 activity was observed for herbicides based on benzoic acid (dicamba), pyridinyloxyacetic acid (triclopyr), or the 6-arylpicolinates (halauxifen), and very low affinity was found for picolinic acid-based auxins (picloram) and quinolinecarboxylic acids (quinclorac).

(4) The atlas demonstrates why some widely used auxin herbicides are not, or are very poor substrates. We list molecular descriptors for AUX1 substrates and discuss our findings in terms of herbicide resistance management.

KEY WORDS

Auxin transport, cheminformatics, herbicide, herbicide resistance, molecular field maps, pharmacophore, structure-activity relationship, uptake carrier.

Introduction

Auxins are increasingly important as agrochemicals, with their primary market as selective herbicides. This market is increasing due to high efficacy, a long history of low environmental impact, just a few instances of resistance (Mithila et al., 2011), the recent introduction of stacked herbicide resistant crops (Behrens et al., 2007; Wright et al., 2010), and a new generation of low field-rate auxins known as the 6-aryl-picolinates (Epp et al., 2016). Despite this, and the wondrous diversity of responses to the endogenous auxin indole-3-acetic acid (IAA), our descriptions for what defines an auxin remain rudimentary. Yet, cheminformatic tools have progressed markedly, and target sites for auxin action have been identified. Past models of auxins have, necessarily, been based on data derived from whole plant bioassays, but it is now possible to access each step in the pathway and generate advanced pharmacophoric maps which may help in the rational design of novel auxins.

Transport proteins are likely to be the first auxin-selective target sites encountered by exogenous auxin applications. The presence of an auxin uptake carrier was first identified from kinetic analyses of auxin accumulation in a variety of systems (Hertel 1983; Hertel et al., 1983; Lomax et al., 1985; Benning 1986; Geier et al., 1990) following development of the chemiosmotic model for auxin transport and accumulation (Rubery and Sheldrake 1974). The energetics of accumulation demonstrated that active indole-3-acetic acid (IAA) uptake was driven by proton cotransport, two protons being required for each IAA^- anion (Lomax et al., 1985; Benning 1986). Little more was learnt about uptake until it was shown that *AUX1* coded for a putative auxin uptake carrier (Bennett et al., 1996). The auxin insensitive 1 (*aux1)* mutant was known to be tolerant to 2,4-dichlorophenoxyacetic acid (2,4-D) and agravitropic (Maher and Martindale, 1980). Subsequent work has then confirmed that AUX1 is an auxin uptake carrier that is

essential for root gravitropism and other morphogenic responses (Marchant et al., 1999; Swarup et al., 2004; Steiger et al., 2002; Bainbridge et al., 2008; Jones et al., 2008), including embryogenesis (Robert et al., 2015).

The AUX1 protein is a member of the amino acid permease, proton co-transporter superfamily (Fischer et al., 1998). A small series of auxin-like molecules were screened as potential inhibitors of uptake and efflux using tobacco cell suspension cultures (Delbarre et al., 1996; Imhoff et al., 2000). Tritiated 2,4-D was shown to be a strong, AUX1-selective substrate, and inhibition of efflux using 1-naphthylphthalamic acid (NPA) allowed a 2-dimensional model of AUX1 substrates to be presented (Imhoff et al., 2000). Expression of AUX1 in *Xenopus* oocytes (Yang et al., 2006) and insect cells using baculovirus (Carrier et al., 2008) confirmed the pH-dependence of uptake, low micromolar estimates of affinity, and affirmed the substrate preference for IAA and 2,4-D. None of these experiments covered the full range of compounds with auxin activity, including a number of scaffolds on which commercially important herbicides are based, including the benzoates, picolinates, and quinolinecarboxylates.

Early decades of auxin research were led by advances in chemistry, using whole-plant bioassays for developing structure-activity relationships (SARs) to account for the hormonal activities of natural and synthetic auxins (Napier, 2001). The drive for new drugs has driven medicinal chemistry to develop advanced chemical informatics tools. Amongst the more widely used are molecular similarity indices that are based on advances in physical parameterisation of molecules. These tools need accurate biological data to build useful pharmacophoric maps (Kaserer et al., 2015). In this report several families of compounds with distinct chemical scaffolds have been screened for AUX1 substrate activity, adding to earlier substrate preference listings (Imhoff et al., 2000). Based on an optimized molecule screening assay and derivation of

a mathematical Competitive Transport Model, accurate AUX1-related transport parameters were then combined to generate pharmacophoric molecular field maps of AUX1 selectivity.

Materrials and Methods

Plant material and auxin herbicides

Arabidopsis thaliana ecotypes Wassilewskija (*Ws*) and *Landsberg erecta* (Ler) were used as controls according to the mutant lines being assayed. The loss-of-function line *aux1-T* was derived from transposon insertion into *Ws*, null allele *wav5-33* and partial loss-of-function line *aux1-2* were derived from Ler (Marchant and Bennett, 1998). Full sequences for each mutant allele have been obtained and confirm that the basis of the phenotype lies within the *AUX1* gene and further phenotypic data is presented elsewhere (Swarup et al., 2004). Auxins and other compounds were the purest available Sigma Aldrich, UK. DAS534 and halauxifen (the product is formulated as Arylex™) were gifts from Dow Agrosciences, Indianapolis, USA.

Root growth bioassays

Arabidopsis thaliana ecotype Wassilewskija (*W*s) and *aux1-100* mutant seed lines were spotted onto 1.5% agar with half strength Murashige and Skoog medium plus 0.5% sucrose, and stratified in the dark at 4°C for 48 hours. After 6 days at 12 h 22°C day and 12 h 18°C night, seedlings were transferred onto serial dilution plates in the same medium, and the position of the primary root tip was marked. Plates were placed vertical for a further 4 days, before being scanned and root growth from the marked point was measured in Image J (Schneider et al., 2012). The dose response curves were fitted to a non-linear regression model of [inhibitor] vs. response – Variable slope (four parameters) using a least squares (ordinary fit) with constrains of 0cm for the bottom value and 2.5cm as the maximum to yield an IC_{50} value (GraphPad Prism v7). Each Y value was considered as an individual point with no weighting applied. Confidence intervals were set at the 95% level. For each compound we compared the best independent fit between the *Ws* and *aux1-100* with a null hypothesis that the IC_{50} is the same, and the alternative

hypothesis being that the IC_{50} is different for each data set. An Extra sum-of-squares F test comparison method was used to reject the null hypothesis for P values less than 0.05.

Accumulation assays

The accumulation of radiolabelled 2,4-D by BY-2 tobacco cell culture cells was measured as described in Hošek et al. (2012). To calculate accurate inhibition constant (IC_{50}) values for a range of auxins and analogues the setup of the accumulation assays was adjusted. [^{3}H]2,4-D was accumulated in the presence of 0, 1, 3, 10, 30 and 100 μM of each tested compound in three repetitions. Samples were collected precisely 1 min and 2 min after the addition of [^{3}H]2,4-D. To allow for the optimisation of [^{3}H]2,4-D diffusion parameters, for each batch of compounds 12 min accumulations were run in the presence of 30 μM CHPAA and 10 μM NPA and samples were collected each minute.

Mathematical modelling

The original model of [^{3}H]2,4-D transport in BY-2 tobacco cells (Hošek et al., 2012) was modified (i) by adding a Michaelis-Menten representation of competition on AUX1-mediated influx, (ii) by adding a representation of extracellular contamination with the tracer from the media that is linearly proportional to the extracellular tracer concentration, and (iii) by omitting the representation of NPA-sensitive efflux, which was blocked with NPA in all assays. By neglecting the contribution of the [^{3}H]2,4-D itself to the saturation of influx, a final ordinary differential equation of the model was obtained (Methods S1a, b) and analytically solved (Methods S1c). The diffusion-only variant of the model was derived from the final solution by substituting zero for Vmax, thus eliminating the terms appropriate to AUX1-mediated influx from the equation. The model was implemented and optimized in MATLAB (The MathWorks

Inc., Natick, MA), the optimization was carried out by a least-square method using the optimization toolbox.

Cheminformatics

Details about compounds were compiled into Data Warrior (http://www.openmolecules.org) using the inbuilt features to calculate many molecular descriptors. Some additional features were calculated using Marvin (http://www.chemaxon.com). Forge is distributed by Cresset, UK. Marvin was used for drawing, displaying and characterizing chemical structures, substructures and reactions. Calculator Plugins were used for structure property prediction and calculation Marvin v15.10.12.0, 2015, ChemAxon (http://www.chemaxon.com). Structures were viewed using the PyMOL Molecular Graphics Systemm (MacPyMol for Mac OSX, 2006 version DeLano Scientific, LLC).

Results

Wild-type and aux1 mutants are differentially-sensitive to most auxin compounds, however, many auxin herbicides are not substrates for AUX1.

The *aux1* 2,4-D-insensitive mutants of *A. thaliana* (Maher and Martindale 1980; Yamamoto and Yamamoto 1998; Swarup et al., 2004) provide the framework for an *in vivo* assay for AUX1 substrate specificity. We used the *aux1* knockout line *aux1-100* and its wild-type line *Wassilewskija* (*Ws;* Figure 1, Supplementary Figure 1), and the knockout *Wav 5-33*, partial loss of function allele *aux 1-2* and their wild-type *Landsberg erecta (Ler;* Supplementary Figures 2 and 3). As anticipated, *AUX1* knockout seedlings showed a resistance to 2,4-D (Figure 1b) and to applied IAA (Figure 1a), but not to 1-NAA (Supplementary Figure 2b). We then tested several classes of synthetic auxins that are used as commercial herbicides (Figure 1c, d, Supplementary Figure 1) and quantified their effectivity in *Ws* and *aux1-100* in terms of growth IC_{50} values (Table 1). The substituted benzoates such as dicamba (3,6-dichloro-2-methoxybenzoic acid), the quinolate quinclorac (3,7-dichloro-8-quinolinecarboxylic acid) and the picolinate auxins picloram (4-amino-3,5,6-trichloro-2-pyridinecarboxylic acid), and fluroxypyr ([(3,5-dichloro-4-amino-6-fluoro-2-pyridinyl)oxy]acetic acid) were all potent auxins in the assay, inhibiting root growth at low concentrations. However, in each case there was no differential sensitivity recorded between wild-type and *aux1* lines suggesting that these compounds are not transported by AUX1. A number of other auxin analogues were also evaluated (Supplementary Figures 2, 3, 4).

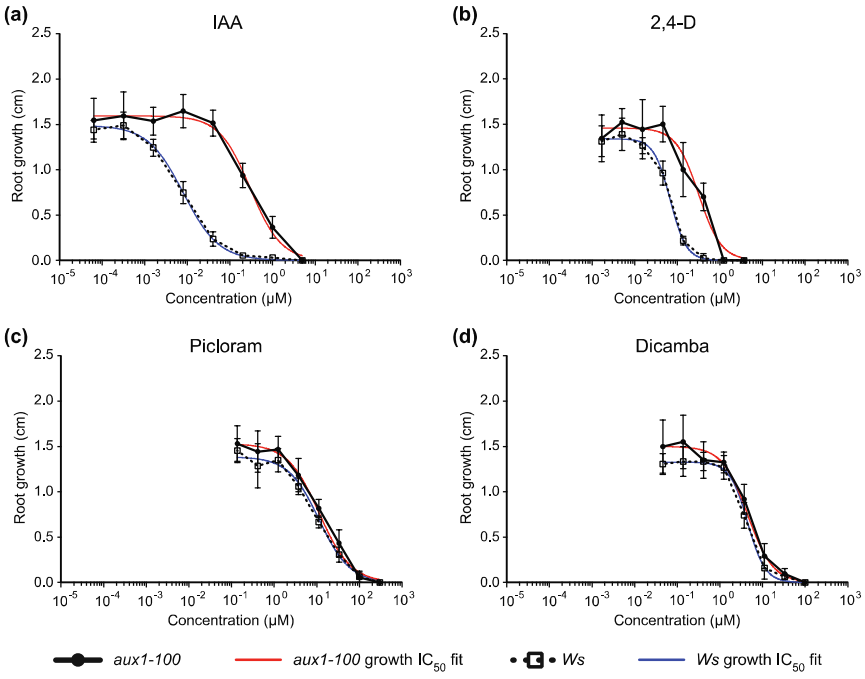

Figure 1. Root elongation dose dependence assays in Arabidopsis lines. Primary root growth of *aux1-100* mutant and wild-type *Ws* lines were recorded after four days on plates holding a dose series of auxin herbicides. (a) IAA, (b) 2,4-D, (c) picloram, (d) dicamba. Values are averaged over 15–20 seedlings and data presented as the mean +/- SE of the mean. Modelled fits were used to calculate IC50 values (Table 1).

Table 1. Estimates of the growth IC_{50} values calculated from Arabidopsis root growth data using *Ws* and *aux1-100* plants.

	WS		*AUX1-100*		P-VALUE (IC_{50} DIFFERS BETWEEN *WS* AND *AUX1-100*)	IC_{50} RATIO (*AUX1-100* / *WS*)
COMPOUND	**IC_{50} (µM)**	**Std. err.**	**IC_{50} (µM)**	**Std. err.**		
IAA	0.008	0.001	0.299	0.032	<0.0001	37.38
2,4-D	0.068	0.036	0.3	0.036	<0.0001	4.41
PICLORAM	10.2	0.911	12.5	1.211	ns	1.23
TRYPTOPHAN	306.5	23.3	504.7	104.6	0.0036	1.65
FLUROXYPYR	2.845	0.297	2.681	0.389	ns	0.94
DICAMBA	4.192	0.216	4.900	0.478	ns	1.17
DAS534	0.502	0.18	0.451	0.149	ns	0.90
CHPAA	45.4	2.734	89.0	5.818	<0.0001	1.96
QUINCLORAC	50.9	3.716	51.8	3.496	ns	1.02
S-DICHLOROPROP	2.425	0.148	9.911	0.827	<0.0001	4.09
R-DICHLOROPROP	0.017	0.002	0.074	0.013	<0.0001	4.35

Parameterisation of an auxin accumulation model using tritiated 2,4-D accumulation assays provides accurate AUX1 substrate affinities.

Radiolabel accumulation into BY-2 tobacco cell suspension cultures has been used as a definitive measure of auxin uptake and efflux since the formative paper of Delbarre et al. (1996). The phenoxy auxin 2,4-D was found to be an excellent substrate for monitoring uptake through AUX1 and thus we used the competitive accumulation of [^{3}H]2,4-D by BY-2 cells in the presence of tested compounds as a measure of their affinity towards AUX1. There have been reports that 2,4-D can also be carried by efflux proteins (Hošek et al., 2012) and possibly ABCB4 as an influx protein (Kubes et al., 2012), and so we included NPA (10 µM) in the assay

to avoid selective dampening of accumulation by active efflux and minimizing an alternative active influx pathway. In our results [^{3}H]2,4-D (2 nM) uptake was competitively inhibited by cold 2,4-D and IAA (Figure 2), which is in agreement with previous reports (Delbarre et al., 1996). Similarly, the known uptake inhibitor 3-chloro-4-hydroxyphenylacetic acid (CHPAA) also showed effective inhibition of tracer uptake (Figure 2c).

In order to quantify the substrate affinities for AUX1 in terms of transport half-saturation concentrations (transport IC_{50} – as opposed to the growth IC_{50} assessed in the root-growth experiment), the compounds in our panel were screened in short-time [^{3}H]2,4-D accumulation assays over a series of compound concentrations (0–100 μM).

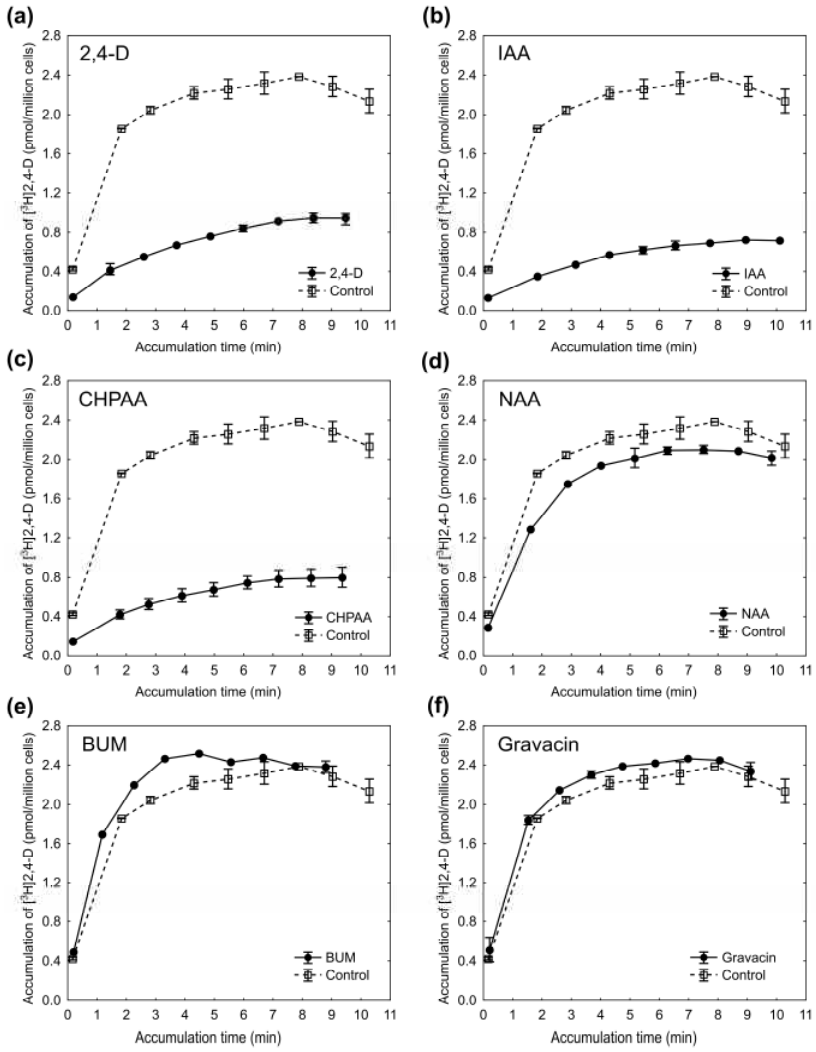

Figure 2. Competitive accumulation assays for a series of auxin-active compounds using tobacco BY-2 cells. Accumulation of [^{3}H]2,4-D is reduced by the addition of unlabelled 2,4-D (a), IAA (b) and CHPAA (c), suggesting that these compounds compete with the [^{3}H]2,4-D for uptake. In contrast, 1-NAA (d) exhibits little or no competition, indicating its poor affinity towards uptake. Similarly, the two auxin efflux inhibitors BUM (e) and Gravacin (f) cause no reduction of tracer accumulation. [^{3}H]2,4-D was applied at a concentration of 2 nM, all competing compounds at 10 µM. Means of two or three independent measurements are shown with their ranges (min–max).

Having optimised the assay, transport IC_{50} values were then obtained by fitting a mathematical model to the resulting competition curves (Figure 3, Table 2). Instead of a simple semi-empirical equation describing competitive accumulation, as used in former studies (Delbarre et al., 1996; Imhoff et al., 2000), a Competitive Transport Model was used for transport IC_{50} estimation. The Competitive Transport Model was derived from our earlier mathematical model of auxin transport (Hošek et al., 2012) that was extended by a more detailed representation of competitively-inhibited AUX1-mediated influx of [^{3}H]2,4-D according to Michaelis-Menten kinetics (see Methods S1 for details). The Model outputs the intracellular concentration of accumulated [^{3}H]2,4-D as a function of: (i) competitor transport IC_{50} and V_{max}, which were optimised for each compound; (ii) competitor concentration and accumulation time, which were both known experimental conditions; and (iii) diffusion parameters of [^{3}H]2,4-D, which needed to be determined before the model could be optimised. In order to obtain diffusion parameters, each batch of screened compounds was accompanied by a longer (12 min) accumulation assay of [^{3}H]2,4-D with active transport inhibited by CHPAA (30 μM) and NPA (10 μM as before). The diffusion parameters were then obtained by optimisation of a modified diffusion-only model using these data, after which our Competitive Transport Model was used to fit the short-time competitive accumulation data using two sampling times in one optimization problem, thus obtaining a single transport IC_{50} estimate valid for both time points. The validity of these IC_{50} estimates (Table 2) is supported by the fact that the ratio of V_{max}/IC_{50} was consistent across the compounds (relative standard deviation 22.3%, Supplementary Figure 5), suggesting both stable performance of the model as well as stable overall efflux activity from the cells throughout the

assays. Similarly, the diffusion parameters obtained for individual screen batches showed reasonable mutual consistency (Supplementary Figure 6).

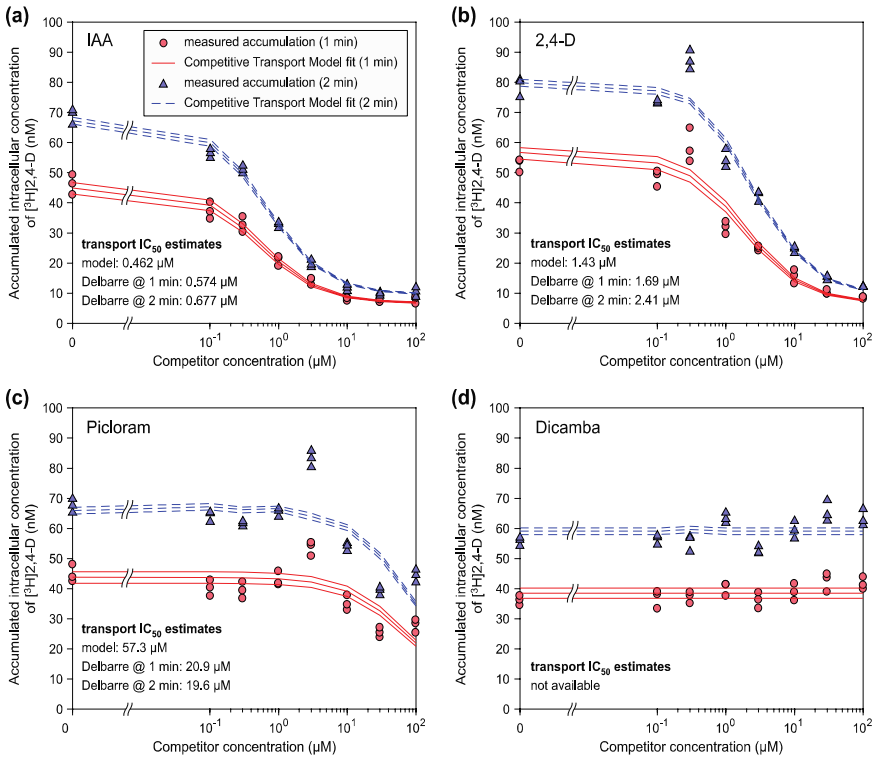

Figure 3. Transport IC_{50} estimations dereived from tobacco cell accumulation assays. The Competitive Transport Model was fitted to [^{3}H]2,4-D accumulation data collected after 1 min (red) and 2 min (blue), in presence of a series of competitor concentrations (0–100 µM). IAA (a) and 2,4-D (b) showed effective inhibition of tracer uptake at low concentrations, thus confirming them to be good AUX1 substrates. On the other hand, picloram (c) and dicamba (d) competed only weakly or not at all (respectively). Transport IC_{50} values estimated by the Competitive Transport Model are shown alongside the estimates made from the same data, but using the semi-empirical model of Delbarre et al. (1996).

Alongside the Competitive Transport Model, we applied the simple semi-empirical equation (Imhoff et al., 2000; Delbarre et al., 1996) and the resulting transport IC_{50} estimates were compared (Supplementary Figure 7). Although somewhat more laborious in its application, the Competitive Transport Model allowed reliable IC_{50} estimations for weak competitors even where full inhibition was not reached within the concentration range tested. In such situations (IC_{50} > ca. 25 µM), the semi-empirical equation struggled as the baseline 'non-saturable component' of the accumulation (mainly diffusion) could not be optimised from the data. Even for stronger competitors (IC_{50} < 25 µM), the semi-empirical equation consistently overestimated the IC_{50} by an average of 50.5% (SD 20.3) in comparison to the Competitive Transport Model (Supplementary Figure 7). However this overestimation was significantly (Wilcoxon Matched Pairs test, $p = 0.0007$, $n = 15$) less serious when samples accumulated for 1 min were processed with the semi-empirical equation (34.2% average overestimation in comparison to the Competitive Transport Model) than in samples accumulated for 2 min (66.9%). Therefore, the 30 s accumulation times used by Imhoff et al. (2000) and Delbarre et al. (1996) were beneficial to the accuracy of their semi-empirical method, making their transport IC_{50} data compatible with our own for further analyses.

In agreement with the seedling root growth assay, many herbicides are not substrates for AUX1. Having established a robust model for accumulation assays, accurate inhibition constant (transport IC_{50}) values were calculated for a range of auxins and analogues (Table 2). The endogenous auxin IAA was found to have the highest affinity for the carrier (lowest IC_{50} concentration, 0.5 µM), with 2,4-D also a very good substrate (IC_{50} = 1.4 µM). Some isomers of

2,4-D had been tested previously (Imhoff et al., 2000), and some of these were rerun to provide a comparative dataset (e.g. Supplementary Figure 3). The commercially-important phenoxypropionates have not been assessed previously and so were included in our current analysis. Assays showed clearly that these phenoxy auxins are strong competitive inhibitors of 2,4-D accumulation, suggesting that they are effective substrates of AUX1 (Table 2; transport IC_{50} mecoprop = 1.8 µM; dichlorprop = 1.6 µM).

Many other auxin herbicides had no effect on [^{3}H]2,4-D accumulation (Figures 3 and 4d, Table 2), suggesting that they are not substrates for AUX1. These included quinolinates (e.g. quinclorac), and benzoates (e.g. dicamba; Figure 3d), which is consistent with the results from the primary root growth assay (Supplementary Figure 1g, Figure 1d, respectively). The Competitive Transport Model was able to assign a transport IC_{50} value to picloram (Figure 3c, Table 2), suggesting that it is a weak substrate with an affinity for AUX1 over 100-fold weaker than that of IAA, but other picolinates of the 6-arylpicolinate class, such as DAS 534 and halauxifen, were found not to be substrates (Table 2).

The results of the [^{3}H]2,4-D accumulation screen show good agreement with the observations from the primary root growth assay, where good AUX1 substrates (low transport IC_{50} in the screen) exhibited high increases of resistance in *aux1-100* mutants, while there was little or no change in resistance to poor substrates (Figure 4a). An exception to this coherence was *S*-dichlorprop that, although being a poor AUX1 substrate, showed a significant increase of resistance in the *aux1-100* mutant. This could be attributed to potential isomerization of *S*-dichlorprop into its *R*- enantiomer (very good AUX1 substrate, IC_{50} = 0.89 µM), which could occur within the time scale of the root growth assay, but not in the short-time uptake

experiments. Enantiomerization of dichlorprop in the environment has been reported, although not specifically *in planta* (Katagi, 2012).

Table 2. **Transport IC_{50} value estimates by the Competitive Transport Model from the tobacco cell transport inhibition screen. These inhibition constant data were used to generate molecular field maps for AUX1.**

Scaffold	Compound	Transport IC_{50} (µM)
Pyrene acetic acid	Pyrene-1-acetic acid	4.564
Indoles	IAA	0.462
	4-Cl IAA	1.330
	5-Cl IAA	3.997
	Indole-3-acetaldehyde	118.575
	3-Methyl Indole	no inhibition
	ICA	14.552
	Indole-3-Carbinol	no inhibition
	Indole-3-glyoxylate	4.343
	IPA	1.332
	Tryptophan	no inhibition
	Tryptophol	no inhibition
	Tryptamin	no inhibition
	IPyA	6.671
	Indole-3-lactic Acid	26.402
	IBA	no inhibition
	PCIB	no inhibition
Phenylacetic acids	CHPAA	1.986
Phenoxy acids	2,4-D	1.434
	MCPA	2.233
	2,3,6-T	no inhibition
	2,4,5-T	12.099
	Mecoprop	1.759
	R-Dichlorprop	0.883
	S-Dichlorprop	58.315
	(*R/S*) Dichlorprop (racemic)	1.645
	Fenoprop	8.080
Benzoic acids	Dicamba	no inhibition
	Chloramben	no inhibition
	2,4-DB	26.845
Pyridinyl acids	Triclopyr	no inhibition
Picolinic acids	Picloram	57.325
	Fluoroxypyr	76.789
	DAS534	no inhibition
	Halauxifen	no inhibition

Quinolinic acids	Quinclorac	no inhibition
Benzothiazolin acid	Benazolin	43.221

Together, the results confirm that cellular uptake of several major classes of auxin herbicide is not, or only very weakly, facilitated by auxin uptake carriers. This is illustrated by the looseness of the relationship between their affinity for AUX1 and their effectivity in plants (Figure 4b).

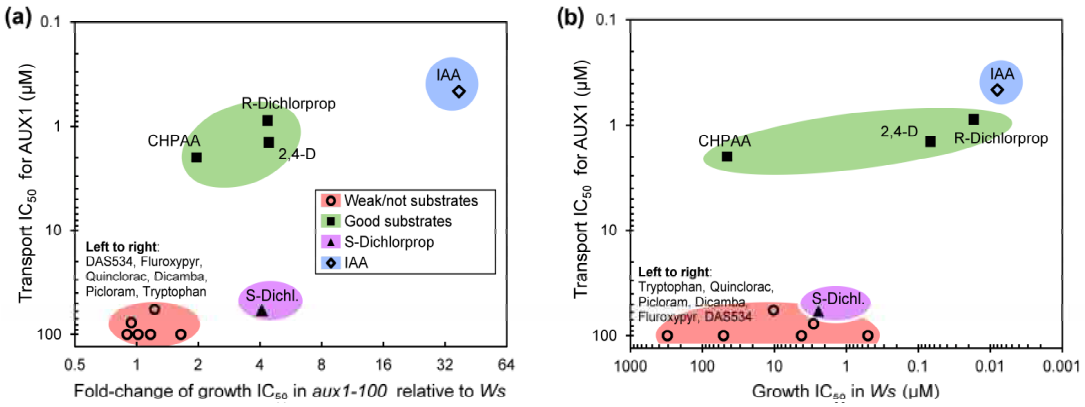

Figure 4. Comparisons of growth and transport IC50 values for selected compounds. The fold-change of Arabidopsis root growth IC_{50} in the *aux1-100* mutant (relative to *Ws*, i.e. the ratio *aux1-100*/*Ws*) corresponds closely with the transport IC_{50} values measured in the tobacco cell radiolabel competition assay (a). Weak substrates (red) showed no notable increase of resistance in *aux1-100*, good substrates (green) exhibited between 2- to 4-fold increase in resistance, and IAA (blue) being by far the best substrate showed a resistance increase of almost 40-fold (Table 1). The exception to this rule was *S*-dichlorprop (magenta) that was significantly more tolerated by the *aux1-100* mutant despite being a poor substrate of AUX1 (transport IC50 = 58.3 µM). In contrast, the relationship between the compound's affinity for AUX1 and its absolute activity in terms of root growth inhibition (in *Ws* plants) is much looser (b). There is considerable overlap in their biological effectivity even though they are well-separated on thy Y-axis by transport IC_{50}.

Arylcarboxylate indoles reveal high AUX1 selectivity for an acetyl side chain and limitations in the seedling bioassay.

A comparison of the capacity of AUX1 to transport the 3-arylcarboxylate series of indoles suggested a distinct selectivity for the 2 carbon acetate side-chain of IAA in the root growth assay (Supplementary Figure 2c–f). The null allele line *wav5-33* showed greatly increased resistance to IAA (Supplementary Figure 2d), but none for indole-3-carboxylic acid, -propionic acid or -butyric acid. However, indole-3-carboxylic acid had no auxin activity (no inhibition of root growth even at high concentrations), and so it is null in the assay.

The indolic amino acid tryptophan is another compound for which the root assay for *aux1* resistance is null. Such null results show that the differential growth bioassay is limited, as may be anticipated given that it requires an auxin-driven response as read-out. Reporter assays using e.g. DR5-driven enzyme or fluorescence activity will be restricted in the same manner. The accumulation assay requires no such auxin response, and it was possible to measure IC_{50} values for the 3-arylcarboxylates. The accumulation data show a clear preference for IAA (IC_{50} = 0.5 µM), but ICA (14.6 µM) and IPA (1.3 µM) were both found to be AUX1 substrates too. The 4 carbon aryl side-chain IBA was not a substrate, and tryptophan was confirmed not to be a substrate (Table 2; Marchant et al., 1999), nor was tryptophol.

Precursors of IAA and other indoles

The metabolic precursors of IAA, indoleacetaldehyde (IAAld), indolepyruvic acid (IpyA) and indoleacetonitrile (IAN) were all tested as substrates for AUX1 using the root growth assay

(Supplementary Figure 4), and the activity plots showed resistance in *aux1-T*, suggesting each was a substrate. However, one other limitation of the root growth assay is the duration of treatment. We considered the possibility that each compound might diffuse into the cell, become converted to IAA which is then transported out via the efflux carrier. This compound-derived IAA load could then both inhibit growth, and be a substrate for AUX1 in adjacent cells. Consequently, for these potential IAA precursor compounds we included the loss-of-function PIN2 mutant allele *agr3* (Muller et al., 1998) to minimise IAA efflux from root cells, both as a control line and in the *aux1/agr3* double mutant. The wild-type background for *agr3* was *Ws* and so *aux1-T* was used for the cross and *Ws* for the control. The loss-of-function *aux1-T* line conferred significant resistance to increasing concentrations of each compound compared to *Ws* and *agr3*. The resistance in the double mutant was reduced in each case, but only for IAN was resistance reduced to levels close to wild-type. Consequently, the data suggested that both IAAld and IpyA are substrates of AUX1. Once again we can turn to the accumulation assays for greater insight, and IPyA was shown to be a reasonably good substrate (IC_{50} = 6.7 µM). Unfortunately IAN and IAAld were not assayed, but other indoles were included. Indoles with side chains no longer than 3 atoms and with hydrogen ion acceptors (indole glycolate, indole lactate, indole pyruvate) were all substrates with low micromolar transport IC_{50} values (Table 2), as were 4- and 5-chloroIAAs.

Molecular similarity indices of AUX1 substrate molecules

The availability of additional SAR data combined with existing data (Imhoff et al., 2000) encouraged us to apply new cheminformatic tools to analyse AUX1 selectivity. We entered the quantitative values into the pharmacophoric software Forge (Cresset plc). Using molecular descriptor analysis features calculated in Data Warrior (openmolecules.org), the compounds are

summarised by physicochemiocal features (Table 3). All conform to Lipinski's rule of five (Lipinski et al., 1997; Lipinski and Hopkins, 2004) and more recent analyses of agrochemical properties (Tice, 2001; Avram et al., 2014).

Table 3. Lipinski-type molecular descriptors for the compounds tested as AUX1 substrates.

No.	Descriptor	Value
1.	Molecular weight	<350 (Lipinski <500)
2.	Number of aromatic rings	<4
3.	H bond Donors	<3 (Lipinski <5)
4.	H Bond Acceptors	<4 (Lipinski <5)
5.	Rotatable Bonds	<4
6.	Octanol-water partition coefficient, log*P*	<4 (Lipinski <5)
7.	pKa	<5
8.	Aqueous solubility, clogS	-2 to -4 log (mol/L)
9.	Polar surface area	15 to 90 $Å^2$

A molecular field atlas for AUX1

A structural model for AUX1 substrate selectivity has stood since 2000 (Imhoff et al., 2000). It is based on the 2-dimensional structural profile of the strong uptake inhibitor pyrene-1-acetic acid. Compounds are compared based on their profile overlap. When aligned by their carboxylic acid groups, active uptake competitors can be superimposed onto the pyrene-1-acetic acid template without projections. Less active competitors generally have electron-rich groups, such as chlorines, protruding past the edges of the template, or polar groups within the large hydrophobic platform of the pyrene ring system, and for many years this model has helped us understand

AUX1 selectivity. We started to map auxins onto the Imhoff model using ChemAxon's Marvin Sketch 3D alignment calculator plug-in, which allows compounds to be modelled in 3-dimensions (Figure 5). Whilst there was agreement in a number of cases, such as for IAA (AUX1 substrate; Supplementary Figure 8a) and picloram (very poor substrate; Supplementary Figure 8b), in other cases fits in the 3-dimensional model failed to reflect substrate effectiveness, such as for the classic substrate 2,4-D (Supplementary Figure 8c). Therefore, we adopted the molecular field mapping approach using Forge software (Cheeseright et al., 2006) which is a suite of computational tools designed to help users understand SARs by generating quantitative, 3-dimensional models of pharmacophore activity.

In order to establish a spatial template for the AUX1 pharmacophore, we selected poses for IAA (PDB code 2P1Q) and 2,4-D (2P1N) from their crystal structures in TIR1 (Tan et al., 2007). These poses are identical to independently ipso-crystallised structures in the Cambridge Structure Database (INACET03 and CPXACA01). We extracted the 3D coordinates for each compound and introduced them into Forge Field Templater as reference structures. The molecular interaction fields for each reference were calculated in Forge which uses field point scoring and field point extrema, rather than quantum chemistry calculations for complete surfaces in order to reduce computational time (Cheeseright et al., 2006). Figure 5 shows field points observed from 2 perspectives. Most field features for IAA and 2,4-D are common, such as hydrophobicity from their aromatic rings (Figure 5a, b), and steric volume (indicated by the van der Waals field maps, Figure 5g, h) with the 2 chlorines of 2,4-D compensating for the lack of a second aromatic ring.

All the compounds from our accumulation set (Table 2) and all non-duplicated compounds from Imhoff et al. (2000) were imported into Forge as a training set, along with their activity data. For

each compound Forge generated an energetically feasible conformer, before aligning this to the reference template. Compounds were given equal weighting for field and shape similarities, which gave good alignments and overlaps between their interaction fields and structural features. Each alignment was visually inspected against the reference compounds to ensure conformers and alignments were plausible. An activity atlas was generated in a series of 3D maps, linking activity data to the template and revealing features promoting or compromising affinity (Figure 6).

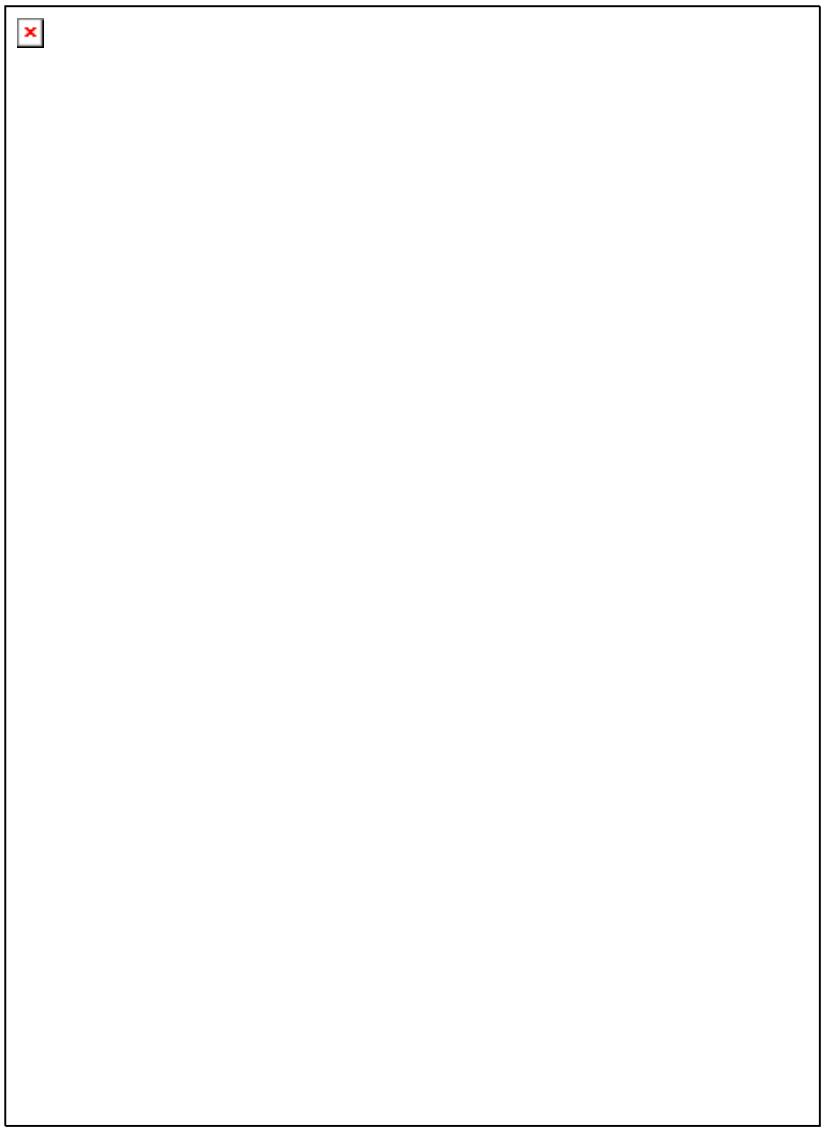

Figure 5. Forge-generated field point map features for IAA and 2,4-D. Crystal structures were overlaid for IAA (grey) and 2,4-D (dark grey) with field points spherical and octahedral, respectively, and sown from above (left panels; a, c, e, g) and the side (right panels; b, d, f, h). Maps are shown for hydrophobicity (a, b), negative electrostatics (c, d), positive electrostatics (e, f) and shape (van der Waals; g, h). The size of each field point symbol represents the strength of that property. Note the consistency between the hydrophobic, negative electrostatic and van der Waals force maps, with most spheres and octahedrons appearing close to each other. In the positive electrostatics, note the absence of an octahedral (2,4-D) field point adjacent to strong sphere adjacent to the indole nitrogen of IAA.

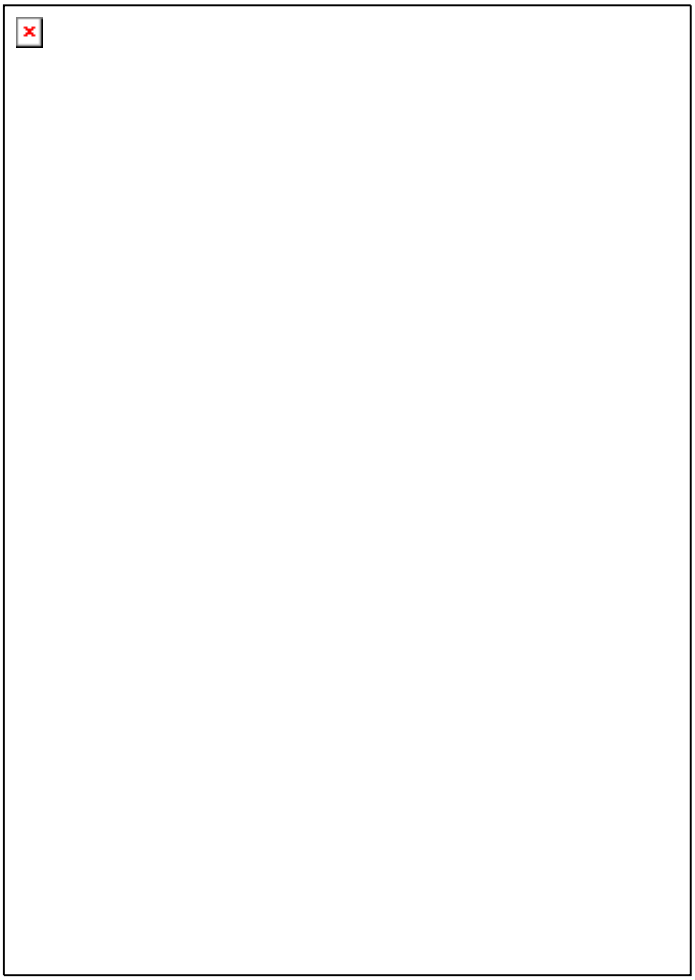

Figure 6. Summary AUX1 molecular field activity maps illustrated with 2,4-D for reference. The average shape map for active substrates is seen from above (a), and from the side (b), and with shape activity cliffs overlaid (c and d). Magenta represents unfavourable, and green favourable space around each activity map. Similarly, the hydrophobicity map is shown (e and f), and together with the hydrophobicity activity cliffs (g and h). In the summary electrostatic molecular field map (i and j), negative charge (blue) surrounds the carboxylic acid moiety as well as areas above and below the aromatic ring. Small areas of positive charge are present adjacent to where the indole nitrogen would sit in e.g. IAA, and adjacent to the α-carbon position.

The molecular field atlas for AUX1 explains why many herbicides are not substrates

The Forge atlas is made up from a series of maps. The AUX1 substrate average shape map indicates that there is space that may be exploited by substrates at e.g. the 3-position of a phenoxy ring (Figure 6a and b) and, perhaps, the 5-position. Overlaying the average shape and shape cliff maps (Figure 6c and d) indicates, for example, that substituents around the side group α-carbon position (Supplementary Figure 9) are favourable as long as they have *R*-chirality (green), whereas substitutions in the *S*-chiral position are unfavourable (magenta). The hydrophobicity map (Figure 6e, f) superimposes well onto the shape map, with unfavourable hydrophobicity activity cliffs at the *S*-chiral α-carbon position and at the 6-phenoxy position (magenta in Figure 6g, h), whereas hydrophobicity at the 3-, 4- and 5- positions is favoured (green).

Examples of the compounds contributing to these rules are *R*- and *S*-dichlorprop. Both enantiomers share the 2,4-dichlorophenoxy ring system, yet affinity is determined by chirality at the α-carbon. The *R*- isomer is the preferred substrate (IC_{50} = 0.88 µM vs *S*-dichlorprop IC_{50} = 58.3 µM) and it can be seen (Supplementary Figure 10) that the chiral methyl group of the *S*-isomer protrudes into the unfavoured shape and hydrophobic activity cliffs, whilst in the R-isomer it projects into favourable space. Elsewhere around the phenoxy scaffold, the substrate shape and hydrophobicity maps show that substitutions at the 6-position reduce activity, with e.g. 2,6-D exhibiting very poor activity (IC_{50} > 300 µM, Imhoff et al., 2000), explained by the hydrophobicity cliff map as the 6-chlorine projecting into a space unfavourable for hydrophobicity (Supplementary Figure 11).

If we consider electrostatic potentials (Figure 6i, j), all auxins are carboxylic acids yielding a core area of electronegativity. The electron-rich areas above and below the aromatic ring system also map as electronegative. There is an electropositive area adjacent to the α–carbon, and the position occupied by the indole nitrogen in IAA. The amine group of picolinates maps to this electropositive area (compare picloram in Figure 7b with the electrostatic activity map in Figure 6i). However, accumulation and root growth assays showed that many herbicides, including the picolinates, are not AUX1 substrates, or are very poor substrates. This is explained by the molecular field maps (Figure 7), which show that these compounds do not fit into e.g. the average shape. Although some contraventions appear small, van der Waals surfaces are not included on the compounds for clarity. Picloram (Figure 7b) extends past the shape boundary by one chlorine, yet this leads to a 100-fold decline in substrate IC_{50} from IAA (Table 2).

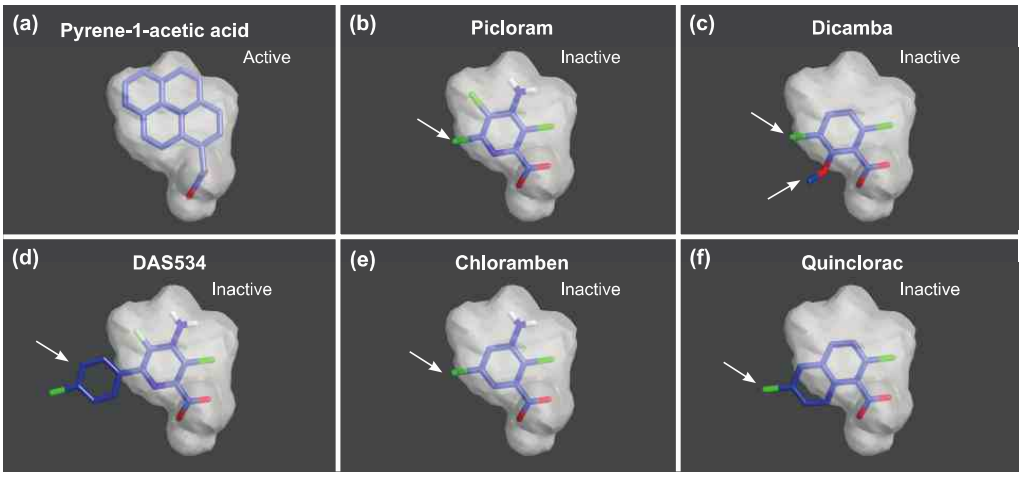

Figure 7. Selected compounds superimposed onto the shape map for AUX1 substrates. Despite its large, conjugated benzene ring system pyrene-1-acetic acid (a) fits within the boundaries of the map and is an effective competitor for 2,4-D accumulation. On the other hand, picloram (b), dicamba (c), DAS534 (d), chloramben (e) and quinclorac (f) are not substrates. It can be seen that each of the latter molecules project partially out of the limits of the space map.

Both the data of Imhoff et al. (2000) and our own data (Table 2) indicate that the large, conjugated ring system of pyrene-1-acetic acid is an effective competitor for [^{3}H]2,4-D accumulation. The molecular field maps do not distinguish compounds that are competitive substrates from those that are competitive inhibitors. Both options are consistent with a 1:1 Langmuir interaction. The former would reduce accumulation of label by substituting for the tracer, the latter would bind to the same recognition site, but fail to transit, blocking accumulation of tracer. Hence the field maps describe molecules that bind specifically to AUX1. To distinguish substrates from inhibitors we will need an assay that can follow the transit of every compound into the cell, not just the reduced accumulation of labelled 2,4-D. Nevertheless, the molecular field maps do reflect a lack of uptake for many auxin herbicides through AUX1. Whilst pyrene-1-acetic acid is large and permitted (Figure 7a), the larger picolinates such as DAS534 (Figure 7d), are not substrates. In this case it is seen that chlorine groups at the two opposite ends, as well as the polar amine group all protrude from the space envelope. Indeed, even the small picloram fails (Figure 7b). Similar observations can be made for benzoates (e.g. chloramben, Figure 7e) and quinolates (e.g. quinclorac, Figure 7f). In conclusion, the 3D molecular field atlas for AUX1 appears to explain substrate activity very well.

Discussion

Structure-activity assays have been used to extend the chemical search space for AUX1 substrate specificity. The differential seedling root growth assay is helpful, but it depends on the test compound having auxin activity. Due to the duration of treatment it may also suffer from

distortions arising from compound metabolism. Nevertheless, this assay did suggest that several classes of synthetic auxin were not transported by AUX1. In order to get accurate and direct estimates of substrate activity for a larger range of compounds, the widely accepted tobacco BY-2 cell suspension accumulation assay was adapted so that we could incorporate Michaelis-Menten kinetics and derive terms to account fully for diffusion. The resulting Competitive Transport Model compared favourably with the more traditional, empirical approach, revealing benefits in terms of accuracy and range, particularly with competitors of lower affinity. Quantitative SAR data for accumulation of [3H]2,4-D in competition with each test compound defined the structural preferences of AUX1, and illustrated that several classes of auxin herbicide are not substrates for this uptake carrier.

In the past several heterologous expression systems have contributed estimates of the affinity of AUX1 for IAA and a few other substrates. Xenopus oocytes yielded uptake kinetics with a Michaelis constant (Km) for IAA of 0.8µM (Yang et al., 2006), and a baculovirus system gave an equilibrium dissociation constant for IAA binding (Kd_{IAA}) of 2.6 µM (Carrier et al., 2008). These values may be compared to IC_{50} values for IAA from plant cells of 0.6 µM (Imhoff et al., 2000), 0.45 µM (Table 2) and 1–5 µM (Rubery and Sheldrake, 1974). For 2,4-D, other estimates of affinity are $IC_{50\ 2,4\text{-}D}$ = 40 µM from baculovirus-infected insect cells (Carrier et al., 2008), 3.3 µM from plant cells (Imhoff et al., 2000) and 1.4 µM (Table 2). Only the study of Imhoff et al. (2000) and the current work have attempted a quantitative SAR survey, although some of these compounds have been evaluated qualitatively as substrates and inhibitors in a number of publications. Consistent with the data reported here, IBA was not a substrate in the Xenopus assay (Yang et al., 2006), nor in a previous report using tobacco (Simon et al., 2013). Also, 1-naphthoxyacetic acid (1-NOA), 2-NOA and CHPAA are competitive inhibitors of AUX1

(Imhoff et al., 2000; Parry et al., 2001; Ottenschläger et al., 2003; Lankova et al., 2010), and the alkyloxy auxins inhibit all auxin transporter systems including AUX1 (Tsuda et al., 2011). Overall, this survey has shown that the uptake carrier AUX1 has considerable selectivity, greater than that shown by the receptors TIR1 and AFB5 for example (Lee at al., 2014). Both assay formats demonstrate that active herbicidal auxins of the benzoic acid, quinolinic acid and picolinic acid families are not substrates of AUX1, or only very weak substrates (Table 2, Figure 4b). Hence, AUX1 does not contribute to the activity of these herbicides. Despite this, the compounds remain effective and some of the picolinates have very low effective field dose rates (Epp et al., 2016). A list of summary rules governing AUX1 substrates is presented (Supplementary Table 1, 2).

Recent advances in cheminformatics have presented chemists, pharmacologists and biologists with ever more powerful computational tools for exploring and describing chemical space. We have presented a summary set of physicochemical descriptors which cluster substrates of AUX1 (Table 3), but are not sufficient to define substrates. On the other hand, molecular field maps (Figure 6) are able to define substrate molecules and explain selectivity. Together, these maps and the cheminformatics analysis do reveal features of AUX1 substrates which may be useful in rational design to improve, or moderate uptake of auxins as agrochemicals.

If we consider herbicidal activity with respect to carrier-mediated uptake of auxins, the lack of affinity by AUX1 for many herbicidal compounds shows clearly that AUX1 uptake is not a pre-requisite for accumulation and subsequent death. The work of Delbarrre and colleagues (1996) explained the high activity of 2,4-D by measuring both uptake (excellent substrate) and efflux (poor substrate) kinetics, and the consequent concentration in the cytoplasm relative to extracellular supply. In comparison, 2,4-D is a relatively poor substrate for the auxin receptors

TIR1 and the AFBs, showing in particular fast off-rate kinetics relative to e.g. IAA (Lee et al., 2014). Nevertheless, with constant accumulation the nett response will be supra-optimal and herbicidal.

AUX1 is the dominant route for uptake of IAA into plant cells, accounting for 75% of accumulation activity (Delbarre et al., 1996; Rutschow et al., 2014), a situation common to Arabidopsis and tobacco BY-2 cells (Seifertova et al. 2014). In common with the current debates on drug permeation into cells (Kell and Oliver, 2014; Mendes et al., 2015), it remains unclear exactly how the auxin herbicides which are not AUX1 substrates enter plant cells. Our measurements of diffusive accumulation to parameterise the model illustrate that this term is significant. Following the arguments of Kell and colleagues, this is unlikely to be bilayer lipoidal permeability even though this pathway has been considered or implied as a consistent contributor to auxin accumulation in all transport and accumulation models to date. Instead, the accumulation attributed to our diffusive term should be considered as facilitated diffusion (Mendes et al., 2015) and comprises relatively slow, unspecific, but long-term accumulation through other small molecule transporters (Rutschow et al., 2014).

Clearly, there are features of herbicide behaviour in terms of long-distance transport in xylem and/or phloem, compartmentation, and particularly metabolism, which are not yet fully explained for all the auxins. Intracellular concentration of 2,4-D is recognised, linking it with uptake carrier activity, but it is transported little within plants (McCready and Jacobs, 1963), which is consistent with it being a poor substrate for efflux and polar auxin transport. Yet, sufficient compound is carried through target plants to be lethal over time. Indeed, one instance of field resistence to 2,4-D has been linked with reduced transport from source leaves to sink leaves (Goggin et al., 2016). The mechanistic basis of this resistance is not yet known, but this example

of evolved resistance does demonstrate that impaired long-distance transport can provide resistance. This challenge of distribution and accumulation is still more acute for the auxin herbicides which are not AUX1 substrates and, consequently, may not become concentrated intracellularly in the manner of 2,4-D.

The cheminformatic survey could be extended to allow useful prediction of additional AUX1 substrates or to design carrier–friendly features onto other auxin molecules. Perhaps more importantly, this set of molecular field maps may contribute to a greatly improved understanding of its mechanism of action. There is not crystallographic structure yet for AUX1, although structures for some transport proteins in the same group are now available (e.g. Sun et al., 2014). A structure for AUX1 would be instructive, but without a molecular mechanism for molecule selection and proton-coupling the structure has limited value.

In times when resistance to auxin herbicides is on the increase (Mithila et al., 2011), it is of interest to identify the role played by AUX1 in accumulation of natural and synthetic auxins in order to evaluate the role played by facilitated auxin uptake. By redefining the selectivity profile of AUX1 using molecular field maps, we reflect on the contribution the uptake carrier AUX1 plays in herbicide resistance mechanisms.

In conclusion, a set of molecular field maps (a 3-dimensional pharmacophoric atlas) has been generated from quantitative SAR data for the auxin uptake carrier AUX1. This protein is highly selective and cheminformatic analysis has contributed new insights to the systemic movement of auxins in plants. Several families of commercially important auxins are not substrates, or are very poor substrates of AUX1 and this information contributes to the discussion on mechanisms of auxin herbicide accumulation and resistance.

Acknowledgements

We are grateful to Dr Terry Walsh and Dr Jared Bell at Dow AgroSciences (Indianapolis, USA) for providing samples of the picolinate herbicides used in this work.

Conflicts of Interest. "The authors declare that they have no conflict of interest."

REFERENCES

Avram S, Funar-Timofei S, Borota A, Chennamaneni SR, Manchala AK, Muresan S. 2014. Quantitative estimation of pesticide-likeness for agrochemical discovery. *Journal of Cheminformatics* **6**: 42 - 46.

Bainbridge K, Guyomarc'h S, Bayer E, Swarup R, Bennett M, Mandel T, Kuhlemeier C. 2008. Auxin influx carriers stabilize phyllotactic patterning. *Genes and Development* **22**: 810-823.

Behrens MR, Mutlu N, Chakraborty S, Dumitru N, Jiang W-Z, LaVallee BJ, Herman PL, Clemente TE, Weeks DP. 2007. Dicamba resistance: Enlarging and preserving biotechnology-based weed management strategies. *Scien*ce **316**: 1185–1188.

Bennett MJ, Marchant A, Green HG, May ST, Ward SP, Millner PA, Walker AR, Schultz B, Feldmann KA. 1996. Arabidopsis *AUX1* gene: a permease-like regulator of root gravitropism. *Science* **273**: 948-950.

Benning C. 1986. Evidence supporting a model of voltage-dependent uptake of auxin into *Cucurbita* vesicles. *Planta* **169**: 228-237.

Carrier DJ, Abu Bakar NT, Swarup R, Callaghan R, Napier RM, Bennett MJ, Kerr ID. 2008. The Binding of Auxin to the Arabidopsis Auxin Influx Transporter AUX1. *Plant Physiol*ogy **148**: 529–535.

Cheeseright T, Mackey M, Rose S, Vinter AJ. 2006. Molecular field extrema as descriptors of biological activity: definition and validation. *Journal of Chemical Information and Modelling* **46**: 665-76.

Delbarre A, Műller P, Imhoff V, Guern J. 1996. Comparison of mechanisms controlling uptake and accumulation of 2,4-dichloropenoxyacetic acid, naphthalene-1-acetic acid and indole-3-acetic acid in supension-cultured tobacco cells. *Planta* **198**: 532-541.

Epp JB, Alexander AL, Balko TW, Buysse AM, Brewster WK, Bryan K, Daeuble JF, Fields SC, Gast RE, Green RA, et al. 2016. The discovery of Arylex™ active and Rinskor™ active: Two novel auxin herbicides. *Bioorganic and Medicinal Chemistry* **24**: 362-71.

Fischer W-N, André B, Rentsh D, Krolkiewicz S, Tegeder K, Frommer WB. 1998. Amino acid transport in plants. *Trends in Plant Sci*ence **3**:188-195.

Geier U, Werner O, Bopp M. 1990. Indole-3-acetic acid uptake in isolated protoplasts of the moss *Funaria hygrometrica*. *Physiologia Plantarum* **80**: 584-592.

Goggin DE, Cawthray GR, Powles SB. 2016. 2, 4-D resistance in wild radish: reduced herbicide translocation via inhibition of cellular transport. *Journal of Experimental Botany* **67**: 3223-3235.

Hertel R. 1983. The mechanism of auxin transport as a model for auxin action. *Zeitscript Pflanzenphysiologia* **112:** 81-101.

Hertel R, Lomax TL, Briggs WR. 1983. Auxin transport in membrane vesicles from *Cucurbita pepo* L. *Planta* **157**: 193-201.

Hošek P, Kubeš M, Laňková M, Dobrev PI, Klima P, Kohoutová M, Petrášek J, Hoyerová K, Jiřina M, Zažímalová E. 2012. Auxin transport at cellular level: new insights supported by mathematical modelling. *Journal of. Experimental Bot*any 63: 3815-3827.

Imhoff V, Műller P, Guern J, Delbarre A. 2000. Inhibitors of the carrier-mediated influx of auxin in suspension cultured tobacco cells. *Plant*a **210**: 580-588.

Jones AR, Kramer EM, Knox K, Swarup R, Bennett, MJ, Lazarus CM, Leyser HMO, Grierson CS. 2008. Auxin transport through non-hair cells sustains root-hair development. *Nature Cell Biology* **11**: 78-84.

Kaserer T, Beck KR, Akram M, Odermatt A, Schuster D. 2015. Pharmacophore Models and Pharmacophore-Based Virtual Screening: Concepts and Applications Exemplified on Hydroxysteroid Dehydrogenases. *Molecules* **20**: 22799–22832.

Katagi T. 2012. Isomerization of chiral pesticides in the environment. *Journal of Pesticide Science* **37**: 1-14.

Kell DB, Oliver SG. 2014. How drugs get into cells: tested and testable predictions to help discriminate between transporter-mediated uptake and lipoidal bilayer diffusion. *Frontiers of Pharmacoogy* **5**: 231.

Kubeš M, Yang H, Richter GL, Cheng Y, Młodzińska E, Wang X, Blakeslee JJ, Carraro N, Petrášek J, Zažímalová E, Hoyerová K, Peer WA, Murphy AS. 2012. The Arabidopsis concentration-dependent influx/efflux transporter ABCB4 regulates cellular auxin levels in the root epidermis. *Plant Journal* **69**:640-54.

Lanková M, Smith RS, Pesek B, Kubes M, Zazímalová E, Petrásek J, Hoyerová K. 2010. Auxin influx inhibitors 1-NOA, 2-NOA, and CHPAA interfere with membrane dynamics in tobacco cells. *Journal of. Experimental Bot*any 61: 3589-98.

Lee S, Sundaram S, Armitage L, Evans JP, Hawkes T, Kepinski S, Ferro N, Napier RM. (2014) Defining binding efficiency and specificity of auxins for SCF(TIR1/AFB)-Aux/IAA co-receptor complex formation. *ACS Chemical Biology* **9**: 673-82.

Lipinski C, Hopkins A. 2004. Navigating chemical space for biology and medicine. *Nature* **432**: 855-861.

Lipinski CA, Lombardo F, Dominy BW, Feeney PJ. 1997. Experimental and computational approaches to estimate solubility and permeability in drug discovery and development settings. *Advances in Drug Delivery Reviews* **23**: 3–25.

Lomax TL, Mehlhorn RJ, Briggs WR. 1985. Active auxin uptake by zucchini membrane vesicles: quantitation using ESR volume and ΔpH determinations. *Proceedings of the National Acadamy of Sciences USA* **82**: 6541-6545.

Maher P, Martindale SJB. 1980. Mutants of *Arabidopsis thaliana* with altered responses to auxin and gravity. *Biochemical Genetics* **18**: 1041-1053.

Marchant A, Bennett MJ. 1998. The *Arabidopsis AUX1* gene: a model to study mRNA processing in plants. *Plant Molecular Bi*ology **36**: 463-471.

Marchant A, Kargul J, May ST, Müller P, Delbarre A, Perrot-Rechenmann C, Bennett MJ. 1999. AUX1 regulates root gravitropism in Arabidopsis by facilitating auxin uptake within root apical tissues. *EMBO Journal* **18**: 2066-2073.

McCready CC, Jacobs WP. 1963. Movement of growth regulators in plants II. Polar transport of radioactivity from indoleacetic acid-[^{14}C] and 2,4-dichlorophenoxyacetic acid-[^{14}C] in petioles of *Phaseolus vulgaris*. *New Phytologist* **62**: 19-34.

Mendes P, Oliver SG, Kell DB. 2015. Fitting Transporter Activities to Cellular Drug Concentrations and Fluxes: Why the Bumblebee Can Fly. *Trends in Pharmacological Sciences* **36**: 710 – 723.

Mithila J, Hall CJ, Johnson WG, Kelley KB, Riechers DE. 2011. Evolution of resistance to auxinic herbicides: historical perspectives, mechanisms of resistance, and implications for broadleaf weed management in agronomic crops. *Weed Science* **59**: 445-457.

Müller A, Guan CH, Galweiler L, Tanzler P, Huijser P, Marchant A, Parry G, Bennett M, Wisman E, Palme K. 1998. AtPIN2 defines a locus of Arabidopsis for root gravitropism control. *EMBO Journal* **17**: 6903-6911.

Napier RM. 2001. Models of auxin binding. Journal of *Plant Growth Regulation* **20**: 244–254.

Ottenschlager I, Wolff P, Wolverton C, Bhalerao RP, Sandberg G, Ishikawa H, Evans M, Palme K. 2003. Gravity-regulated differential auxin transport from columella to lateral root cap cells. *Proceedings of the National Acadamy of Sciences USA* **100**: 10096-10101.

Parry G, Delbarre A, Marchant A, Swarup R, Napier RM, Perrot-Rechenmann C, Bennett MJ. 2001. Novel auxin transport inhibitors phenocopy the auxin influx carrier mutation aux1. *Plant Journal* **25**: 399-406.

Petrasek J, Mravec J, Bouchard R, Blakeslee JJ, Abas M, Seifertova D, Wisniewska J, Tadele Z, Kubes M, Covanova M, et al. 2006. PIN proteins perform a rate-limiting function in cellular auxin efflux. *Science* **312**: 914-918.

Robert HS, Grunewald W, Sauer M, Cannoot B, Soriano M, Swarup R, Weijers D, Bennett MJ, Boutilier K, Friml J. 2015. Plant embryogenesis requires AUX/LAX-mediated auxin influx. *Development* **142**: 1-10.

Rubery PH, Sheldrake AR. 1974. Carrier-mediated auxin transport. *Planta* **118**: 101-121.

Rutschow HL, Baskin TI, Kramer EM. 2014. The carrier AUXIN RESISTANT (AUX1) dominates auxin flux into Arabidopsis protoplasts. *New Phytologist* **204**: 536–544.

Schneider CA, Rasband WS, Eliceiri KW. 2012. NIH Image to ImageJ: 25 years of image analysis. *Nature Methods* **9**: 671–675.

Seifertová D, Skůpa P, Rychtář J, Laňková M, Pařezová M, Dobrev PI, Hoyerová K, Petrášek J, Zažímalová E. 2014. Characterization of transmembrane auxin transport in Arabidopsis suspension-cultured cells. *Journal of Plant Physiology*. **171**:429-37.

Simon S, Kubeš M, Baster P, Robert S, Dobrev PI, Friml J, Petrášek J, Zažímalová E. (2013) Defining the selectivity of processes along the auxin response chain: a study using auxin analogues. *New Phytologist* **200**: 1034-48.

Stieger PA, Reinhardt D, Kuhlemeier C. 2002. The auxin influx carrier is essential for correct leaf positioning. *Plant Journal* **32:** 509-517.

Sun J, Bankston JR, Payandeh J, Hinds TR, Zagotta WN, Zheng N. 2014. Crystal structure of the plant dual-affinity nitrate transporter NRT1.1. *Nature* **507**: 73–77.

Swarup R, Kargul J, Marchant A, Zadik D, Rahman A, Mills R, Yemm AA, May S, Williams L, Millner PA, et al. 2004. Structure-function analysis of the presumptive auxin permease AUX1. *Plant Cell* **16**: 3069-3083.

Tan X, Calderon-Villalobos LIA, Sharon M, Zheng C, Robinson CV, Estelle M, Zheng N. 2007. Mechanism of auxin perception by the TIR1 ubiquitin ligase. *Nature* **446**: 640-645.

Tice CM. 2001. Selecting the right compounds for screening: does Lipinski's Rule of 5 for pharmaceuticals apply to agrochemicals? *Pest Management Science* **57**: 3 – 16.

Tsuda E, Yang H, Nishimura T, Ueharaǁ Y, Sakai T, Furutani M, Koshiba T, Hirose M, Nozaki H, Murphy AS, Hayashi K-I. 2011. Alkoxy-auxins Are Selective Inhibitors of Auxin Transport Mediated by PIN, ABCB, and AUX1 Transporters. *Journal of Biological Chemistry* **286**: 2354-2364.

Wright TR, Shan G, Walsh TA, Lira JM, Cui C, et al. 2010. Robust crop resistance to broadleaf and grass herbicides provided by aryloxyalkanoate dioxygenase transgenes. *Proceedings of the National Acadamy of Sciences USA* **107**: 20240–20245.

Yamamoto M, Yamamoto KT. 1998. Differential effects of 1-naphthaleneacetic acid, indole-3-acetic acid and 2,4-dichlorophenoxyacetic acid on the gravitropic response of roots in an auxin-resistant mutant of Arabidopsis, *aux1*. *Plant and Cell Physiology* **39**: 660-664.

Yang Y, Hammes UZ, Taylor CG, Schachtman DP, Nielsen E. (2006) High-Affinity Auxin Transport by the AUX1 Influx Carrier Protein. *Current Biology* **16**: 1123–1127.

Supplementary Information:

Fig. S1 Arabidopsis root elongation dose dependence assays of the aux1-100 mutant and wild-type Ws lines with a series of auxin herbicides. Values are averaged over 15-20 seedlings, +/- SE of the mean. Colour codes for data and statistical fits are indicated, lower right.

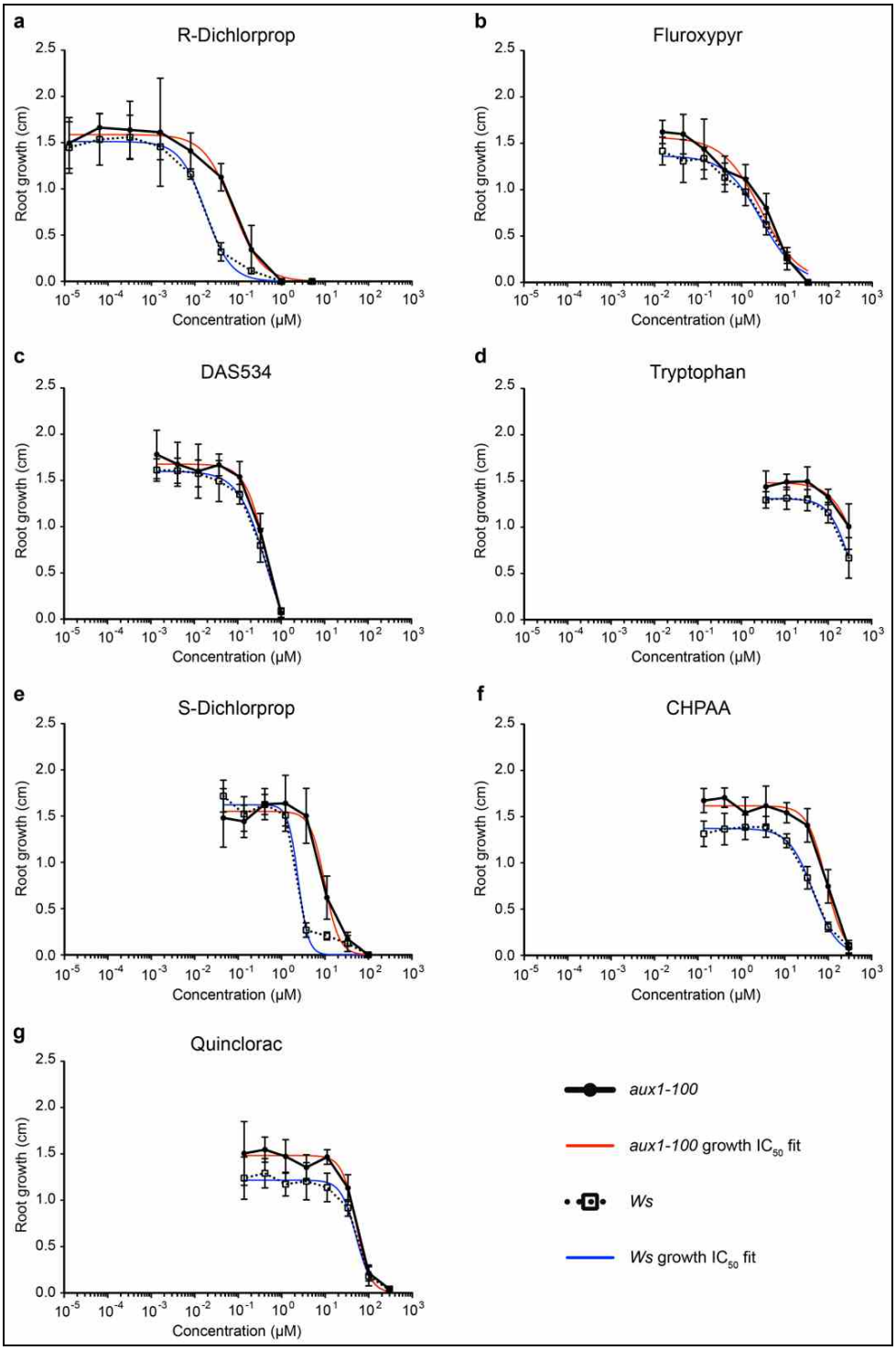
a
R-Dichlorprop
b
Fluroxypyr
c
DAS534
d
Tryptophan
e
S-Dichlorprop
f
CHPAA
g
Quinclorac
Root growth (cm)
Concentration (μM)
aux1-100
aux1-100 growth IC50 fit
Ws
Ws growth IC50 fit

Fig. S2 Arabidopsis root growth dose response curves showing tolerance to 2,4-D (a), but not to 1-NAA (b), and for a series of indole-3-aryl acetic acids (c-f). Data are shown from the lines aux1-T (-○-) and its wild-type Ws (-●-; top panels), and using loss-of-function line aux1-2 (-○-), partial-loss-of-function line Wav5-33 (-▼), and their wild-type line Ler (-●-) in panels C-F. Values are expressed as percentages of root elongation in that line in the absence of compound, averaged over 15-20 seedlings, +/- SE of the mean.

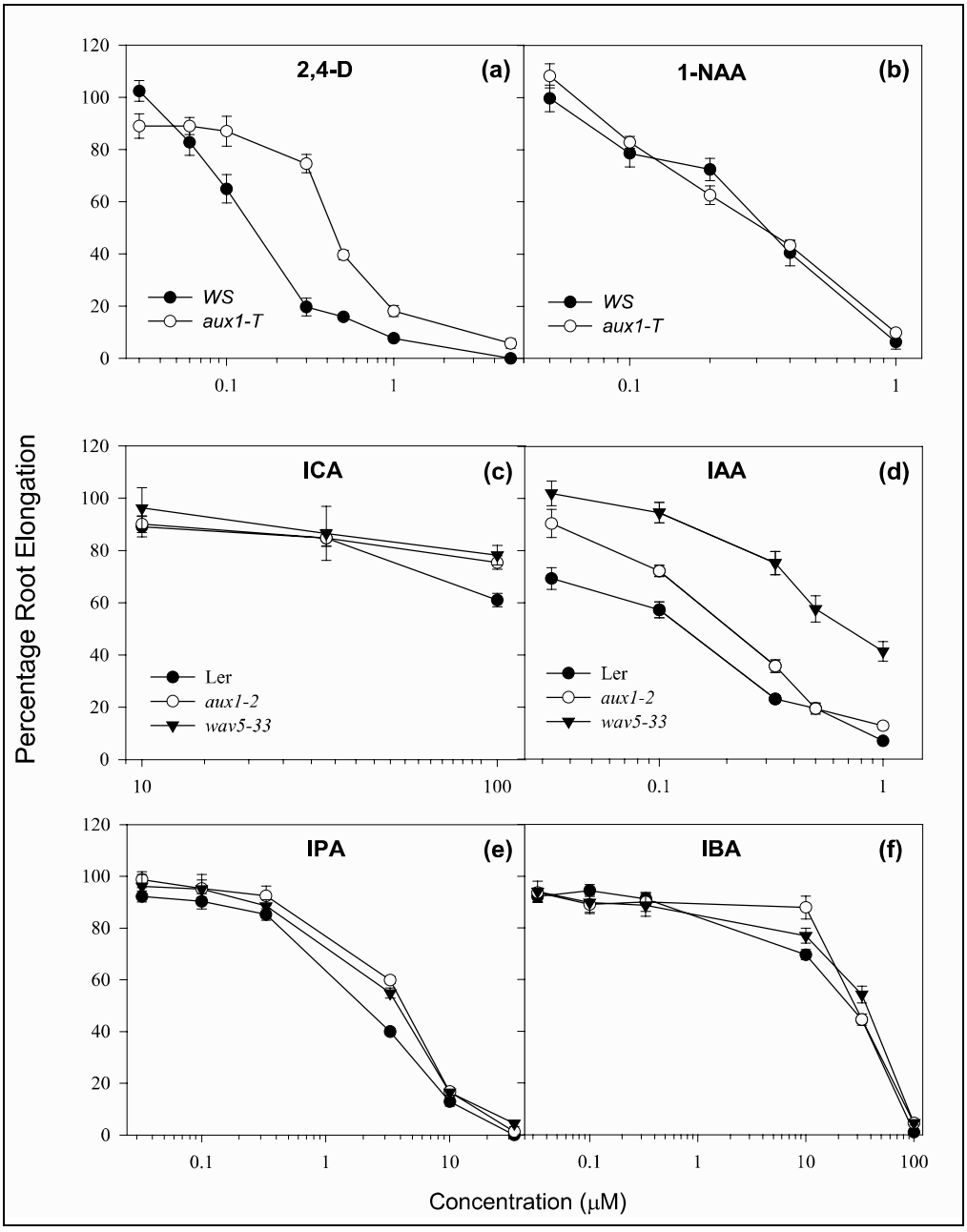

Fig. S3 Arabidopsis r**oot growth dose response curves showing tolerance to some 2,4-D isomers**. Data are shown from the loss-of-function line aux1-2 (-○-), partial-loss-of-function line Wav5-33 (-▼), and their wild-type line Ler (-●-). Values are expressed as percentages of root elongation in that line in the absence of compound, averaged over 15-20 seedlings, +/- SE of the mean.

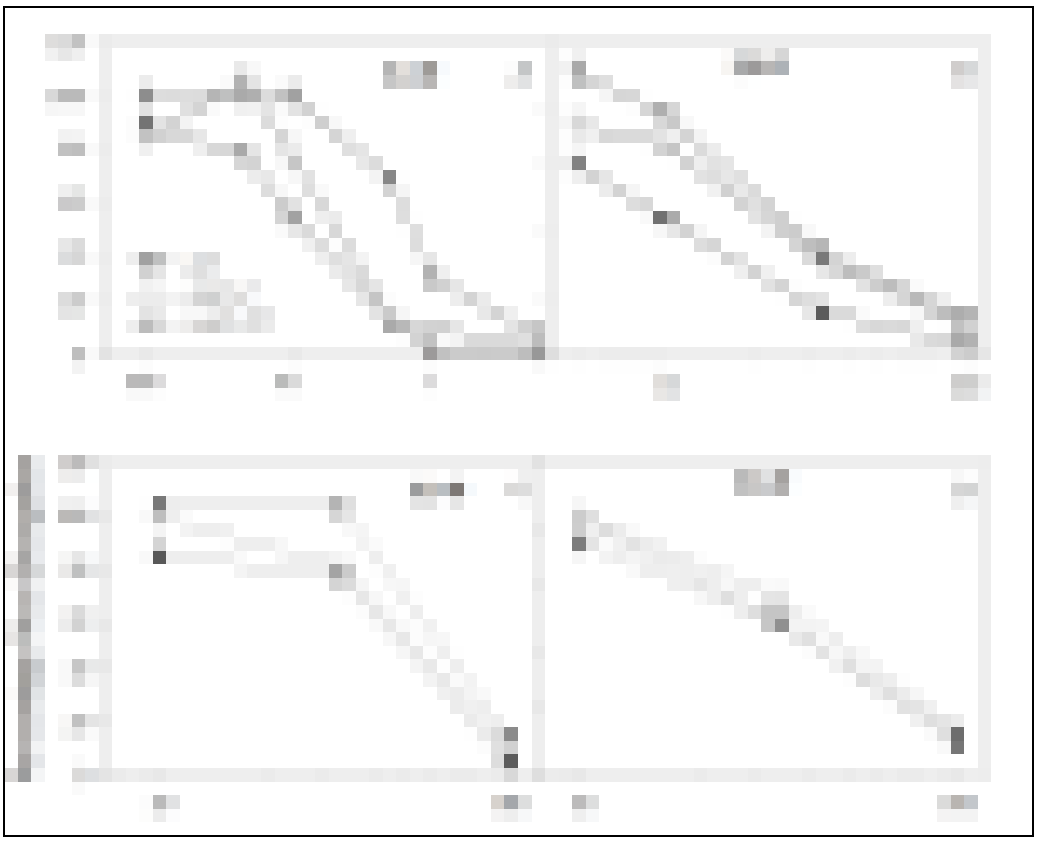

Fig. S4 Arabidopsis root growth dose response curves showing tolerance to some auxin metabolic intermediates. Data are shown from the lines aux1-T (-o-) and its wild-type WS (-●-), supplemented with the auxin efflux carrier mutant agr3 (-▼; Bell and Maher, 1990) and a double mutant aux1-T/agr3 (-◊-). In each case, the tolerance shown in AUX1 knock-out lines was not corrected by loss of PIN2 efflux activity and may be attributed to the loss of uptake activity.

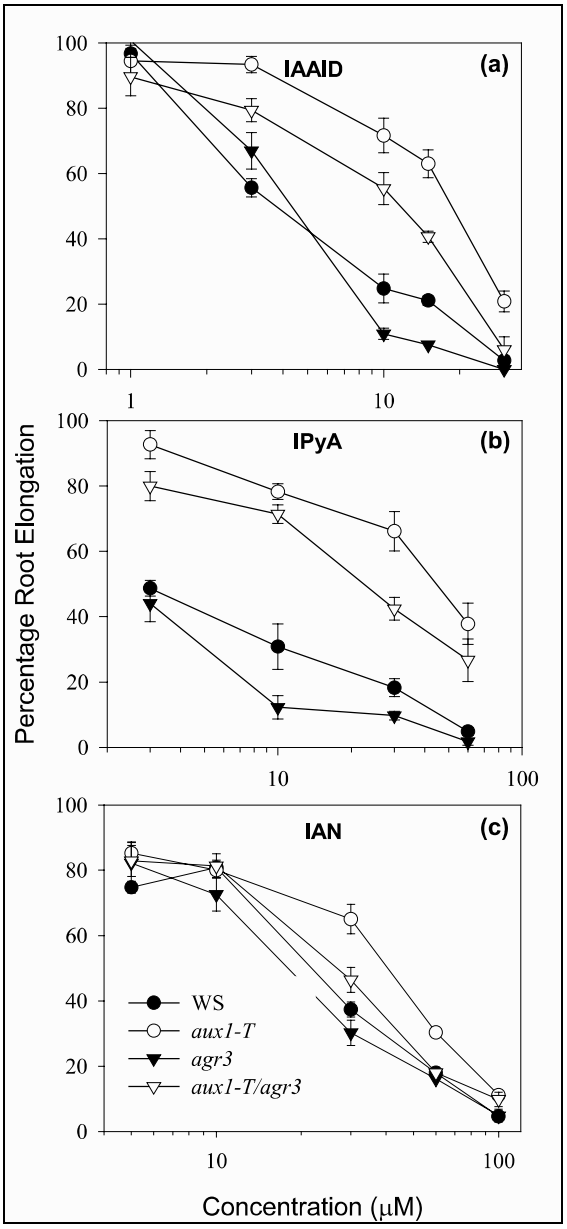

Fig. S5 Log-log scatter plots of transport IC_{50} and V_{max} estimates produced by the Competitive Transport Model. The fact that the points are close to the fitted line (dashed line, fixed zero intercept) reflects that the ratio of V_{max} / IC_{50} was close to constant between compounds. Left – values for all compounds; right – reasonable competitors (IC_{50} < 40 µM) only.

Commentary: It may seem counter-intuitive that the V_{max} estimates themselves are not constant throughout the compound screens, but that the V_{max} / IC_{50} ratios are instead. The explanation is that the V_{max} parameter in the model is neither actual Michaelis-Menten maximum transport rate of the compound nor that of the tracer. Instead, as the V_{max} is expressed in terms of tracer accumulation with respect to each test compound, defined as

$$V_{\max} = \frac{IC_{50}}{IC_{50}^{\text{tracer}}} V_{\text{M}} \ ,$$

where IC_{50} is the half-saturation concentration of the test compound, IC_{50}^{tracer} is the half-saturation concentration of the tracer, and V_M is the maximum transport rate of the tracer ([^{3}H]2,4-D) in terms of Michaelis-Menten kinetics. From this we can see that

$$\frac{V_{\max}}{IC_{50}} = \frac{V_{\text{M}}}{IC_{50}^{\text{tracer}}} \ ,$$

where both V_M and IC_{50}^{tracer} are fixed parameters of the tracer compound, and thus their ratio should be stable across the screen, as observed.

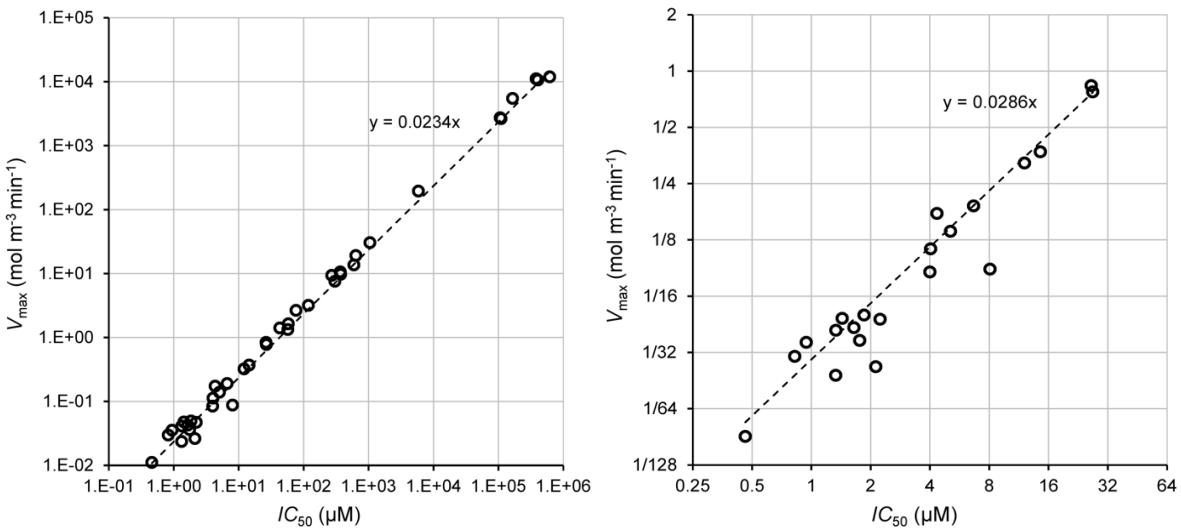

Fig. S6 Comparison of diffusion parameter estimates among screen batches. In the first batch (data0, marked grey), the diffusion was assessed using 4-minute-long accumulation runs; in the remaining batches (black), the duration was optimised to 12 min.

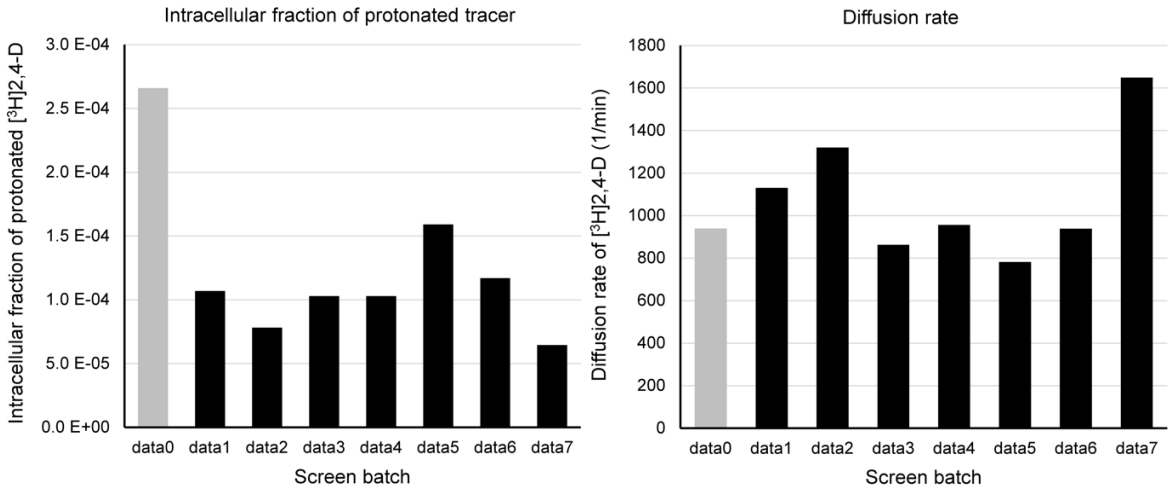

Fig. S7 Comparison of IC_{50} values estimated with the Competitive Transport Model and the estimates made from the same data using the method of Delbarre *et al.* (1996). While the Competitive Transport Model produced one global estimate for both time points, Delbarre's method provided two independent values for each compound. The estimates made by Delbarre's method are consistently higher (by a stable ratio) than the Competitive Transport Model estimates. The estimates from the Delbarre method and 1 min accumulation data are closer to the Model estimates than the 2 min Delbarre estimates.

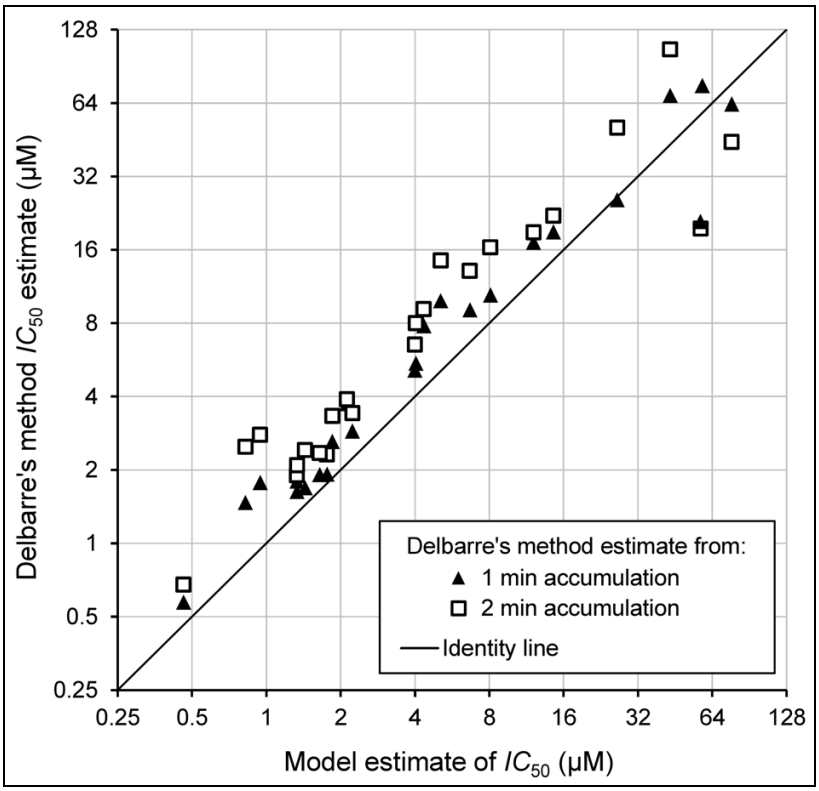

Fig. S8 Numbering of positions on the scaffolds of indole-3-acetic acid (a) and phenoxyacetic acid (b).

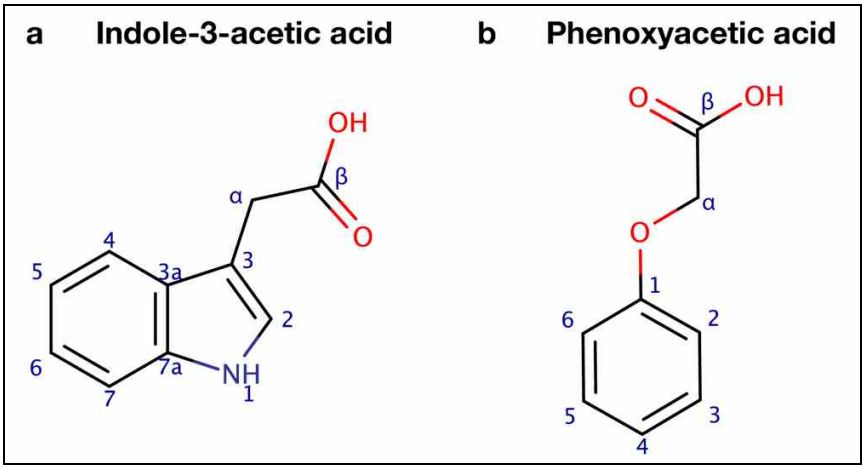

Fig. S9 Representation of the model for AUX1 defined by Imhoff et al. (2000), but using 3-D molecular models (Chemaxon Marvinview). Compounds (dark blue) are aligned with pyrene-1-acetic acid as a template (cyan), in each case viewed from above (left panels) and from the side (right panels). (a) IAA, (b) picloram, and (c) 2,4-D.

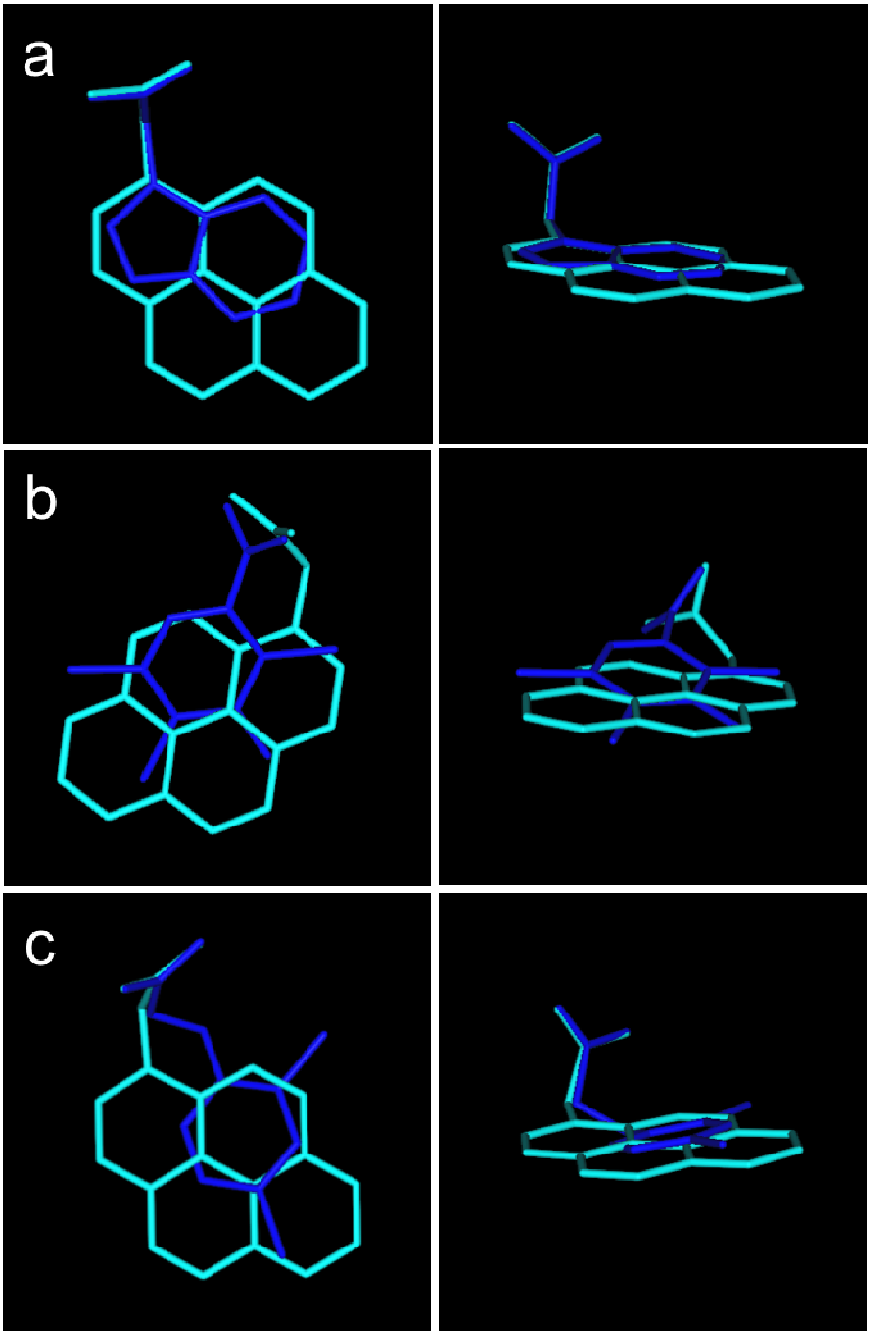

Fig. S10 Molecular field map of AUX1 substrates with dichlorporop enantiomers. The molecular field map of hydrophobicity cliffs shows that the methyl group of S-dichlorprop (S-2,4-dichlorophenoxyisopropionic acid) projects into the unfavourable magenta activity cliff, whereas in the R-isomer it projects out into available space. The methyl groups are shown with non-polar hydrogens (white). The IC50 values for S-dichlorprop are 58.3 µM (our results, Table 2) and 66 µM (Imhoff et al., 2000); while for R-dichlorprop these were 0.88 µM and 2.3 µM (again our results and Imhoff et al., 2000, respectively).

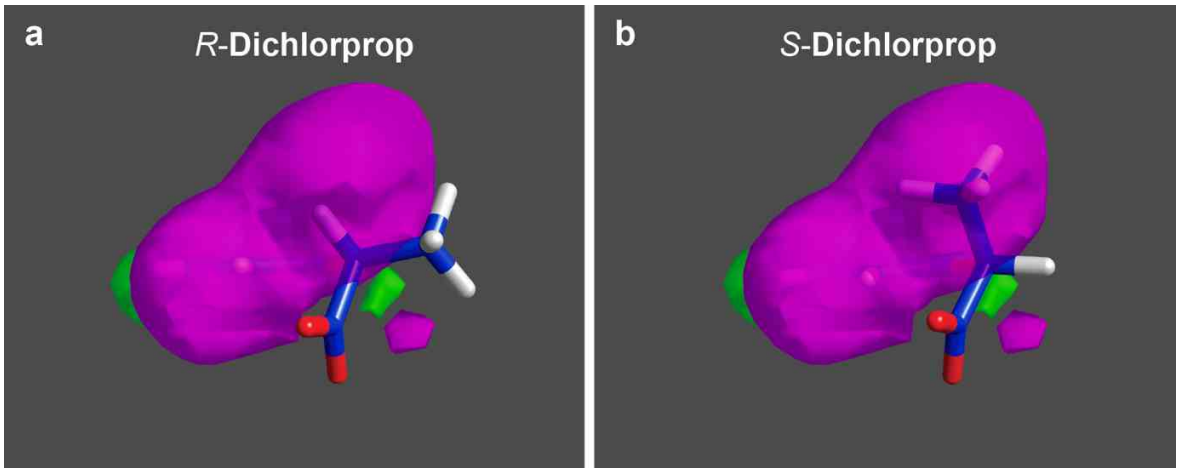

Fig. S11 Molecular field map of AUX1 substrates and substitutions around the phenoxy scaffold. As shown on the example of 2,4,5-T (a), chlorines at the 2-, 4- and 5- positions are not projecting into unfavourable magenta spaces and thus 2,4,5-T is tolerated as a substrate (IC50 = 12.1 µM, Table 2). The non-polar hydrogen at position 6 (a; white) is not computed to project into the unfavourable magenta cloud, in contrast to the larger electronic surface of chlorine in 2,6-D (b; arrowed). 2,6-D is not a substrate of AUX1 (Imhoff et al., 2000).

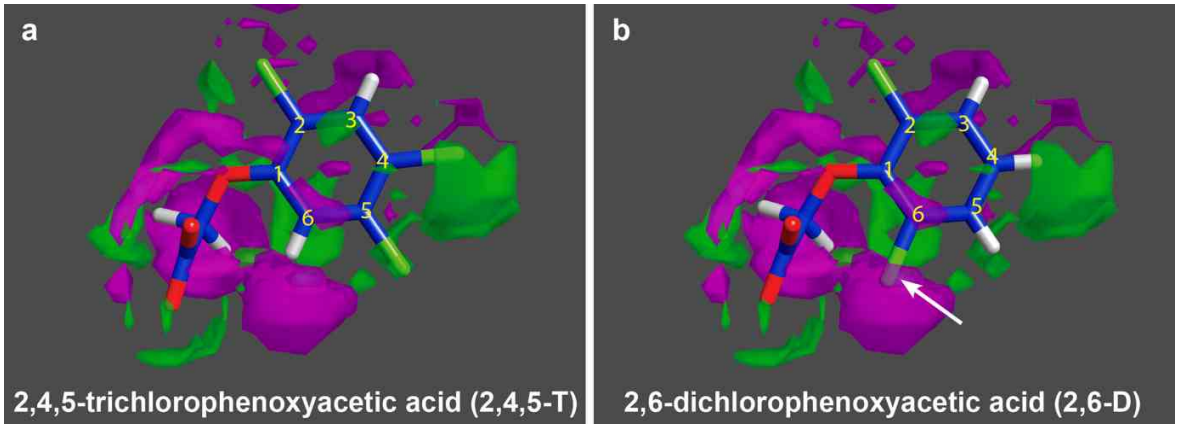

Table S1 Rules for AUX1 substrates

Rule		Description	Rationale
1	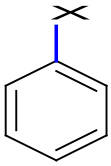	Presence of carboxylic acid and an aromatic ring	Recognition at AUX1 binding site
2	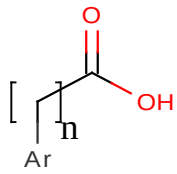	Value for n is 0 or >3	Rotation and space constraints
3	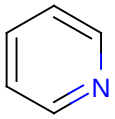	Not pyridine	Hydrogen bond donors/acceptors not compatible with AUX1 recognition site
4	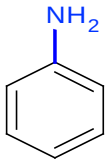	Not aniline	
5	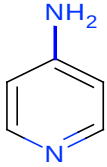	Not pyridin-4-amine	
6	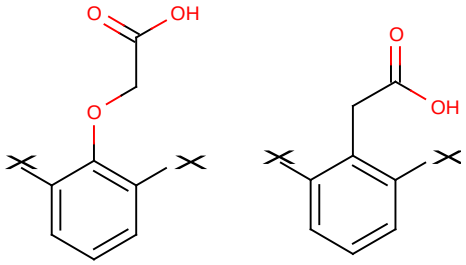	Not di-ortho substituted aromatics	Space and charge constraints
7	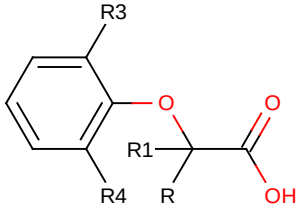 Active IF:	Substituents need to be R- at alpha carbon	Space and hydrophobicity constraints

	R1 and R2 = H and only if R1 or R2 is CH_3		

Table S2 Table of compounds table of rules broken by compounds found not to be substrates

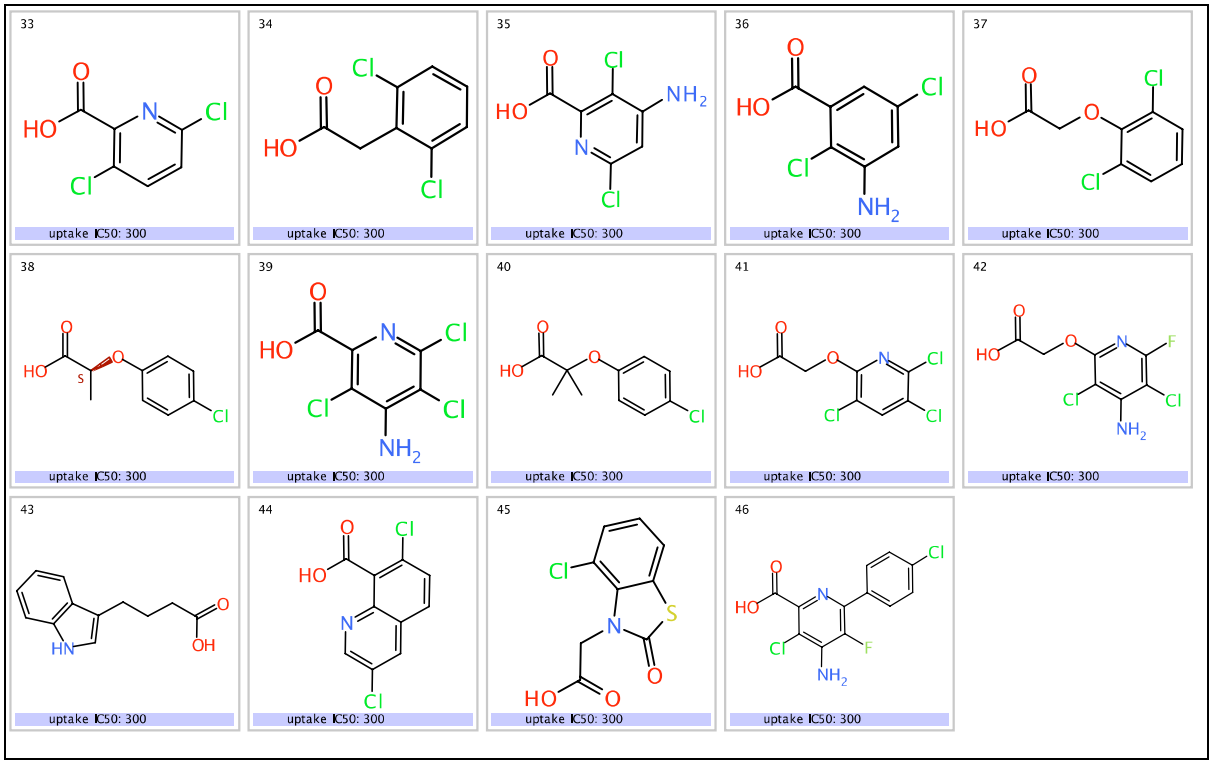

Grid 1: Compounds that break rules

	Rules broken						
Structure no.	2	3	4	5	6	7	Rule 2 = too short; (35, 39, 46, 36, 33, 44,) too long; 43
33	■	■					
34					■		
35	■	■	■	■			Rule 3 = 35, 36, 46, 33, 44 ,42 ,41
36	■	■	■				
37					■		Rule 4 = 35, 39, 46, 36, 42
38						■	
39	■		■	■			Rule 5 =35, 39, 46, 42
40						■	
41		■					Rule 6 = 34, 37
42		■	■	■			
43	■						Rule 7 = 38, 40
44	■	■					
45							
46	■	■	■	■			

Methods S1 The Competitive Transport Model: this mathematical model describes competitively-inhibited AUX1-mediated influx as well as diffusion of [3H]2,4-D.

a: The model is defined by the following two ordinary differential equations describing the dynamics of its state variables: $C_I(t)$ – intracellular concentration of [^{3}H]2,4-D; $C_E(t)$ – concentration of [^{3}H]2,4-D in the medium.

$$\frac{dC_I(t)}{dt} = k_D[p_E C_E(t) - p_I C_I(t)] + \frac{V_{max}}{IC_{50} + C_{comp}} C_E(t)$$

$$\frac{dC_E(t)}{dt} = -\frac{dens \cdot V_C}{1 - dens \cdot V_C} \frac{dC_I(t)}{dt}$$

b: The output of the model – Y(t), which corresponds to the predicted accumulation of [3H]2,4-D in the cells, is then defined as:

$$Y(t) = C_I(t) + k_C C_E(t)$$

c: Final analytical solution of the model

$$\boldsymbol{Y(t, C_{COMP}) = (1 - k_C f) \frac{k_D p_E C_E(0) + \frac{V_{max}}{IC_{50} + C_{comp}} C_E(0)}{k_D p_E f + k_D p_I + \frac{V_{max}}{IC_{50} + C_{comp}} f} \left[1 - e^{-\left(k_D p_E f + k_D p_I + \frac{V_{max}}{IC_{50} + C_{comp}} f\right) t}\right] + k_C C_E(0)},$$

where

$$f = \frac{dens \cdot V_C}{1 - dens \cdot V_C}.$$

d. Table of symbols and units:

Notation	Meaning	Unit
C_E	Extracellular concentration of [^{3}H]2,4-D	mol/m^3
C_I	Intracellular concentration of [^{3}H]2,4-D	mol/m^3
Y	Output of the model, measured accumulation of [^{3}H]2,4-D	mol/m^3
T	Time of accumulation	Min
IC_{50}	IC_{50} of the tested compound	mol/m^3
V_{max}	V_{max} of AUX1-mediated influx of [^{3}H]2,4-D with respect to the tested compound	mol m^{-3} min^{-1}
C_{comp}	Concentration of the competitor, i.e. tested compound	mol/m^3
$Dens$	Suspension density (number of cells per volume of suspension)	1/m^3
V_C	Average volume of one BY-2 tobacco cell	m^3
p_E	Extracellular fraction of protonated [^{3}H]2,4-D	-
p_I	Intracellular fraction of protonated [^{3}H]2,4-D	-
k_D	Diffusion rate constant	1/min
k_C	Cell surface contamination coefficient	-

Colour code:

State variables; Known experimental conditions; Optimised from the diffusion assay; Optimised from the competition assay

SI References:

Bell CJ, Maher EP 1990. Mutants of Arabidopsis thaliana with abnormal gravitropic responses. *Molecular and General Genetics* **220**: 289–293

Delbarre A, Műller P, Imhoff V, Guern J. 1996. Comparison of mechanisms controlling uptake and accumulation of 2,4-dichloropenoxyacetic acid, naphthalene-1-acetic acid and indole-3-acetic acid in supension-cultured tobacco cells. *Planta* **198**: 532-541.

Imhoff V, Műller P, Guern J, Delbarre A. 2000. Inhibitors of the carrier-mediated influx of auxin in suspension cultured tobacco cells. *Plant*a **210**: 580-588.